Diagnosed Three-Dimensional Axisymmetric Structure of the Mulhall Tornado on 3 May 1999

WEN-CHAU LEE

National Center for Atmospheric Research, Boulder, Colorado

JOSHUA WURMAN

Center for Severe Weather Research, Boulder, Colorado

(Manuscript received 16 June 2004, in final form 14 December 2004)

ABSTRACT

On 3 May 1999, an unusually large tornado that caused F4-level damage and killed several people was intercepted by the Doppler on Wheels (DOW) mobile radar near Mulhall, Oklahoma, from a range of 4 to 9 km, resulting in high-resolution volumetric data every 55 s up to 1.5-km altitude over a period of 14 min. For the first time, the evolution and three-dimensional structure of a tornado were deduced using the ground-based velocity track display (GBVTD) technique. After the circulation center was determined, the tangential wind and radial wind were derived from the GBVTD technique at each radius and height. In addition, the axisymmetric vertical velocity, angular momentum, vorticity, and perturbation pressure were deduced from the tangential and radial wind fields. This study focuses on the axisymmetric aspects of this tornado.

The primary circulation of the Mulhall tornado consisted of an 84 m s^{-1} peak axisymmetric tangential wind with the radius of maximum wind (RMW) ranging from 500 to 1000 m. The secondary circulation exhibited a two-cell structure characterized by a central downdraft surrounded by an annular updraft near the RMW. The calculated maximum pressure deficit from a 3-km radius to the tornado center at 50-m altitude was −80 hPa. The maximum vorticity during the first 8 min of observation was located inside the RMW away from the tornado center. This vorticity profile satisfied the necessary condition of barotropic instability. As the tornado weakened afterward, the vorticity monotonically increased toward the center. The computed swirl ratios were between 2 and 6, consistent with the observed multiple vortex radar signatures and the vorticity pattern. Swirl ratios were generally smaller during the weakening phase.

1. Introduction

Tornadoes are one of the most intensely destructive storms in nature. Visually, intense tornadoes are often accompanied by a condensation funnel cloud whose diameter ranges from ~100 to ~2 km. Sometimes, multiple (suction) vortices are embedded within larger tornadoes where the maximum damage is generally associated with unsteady peak velocities adding to the mean tornado velocity (e.g., Fujita 1970; Fujita et al. 1970). However, the extreme wind speeds within a tornado are estimated primarily from analyses of structural damage [e.g., the F scale; Fujita and Pearson (1973); Marshall (2004); and early work by Letzmann (1923) as reported by Peterson (1992a,b)], not by direct measurement of the wind. Tornado wind speeds have also been estimated by tracking debris and cloud tags in consecutive frames taken by movie cameras (e.g., Hoecker 1960; Golden and Purcell 1978). The maximum tangential wind in the Dallas tornado (2 April 1957) derived from this method was ~75 m s^{-1} at a radius of ~40 m and an elevation of 70 m (Hoecker 1960) while the maximum tangential wind was ~80 m s^{-1} at a radius of ~200 m and an altitude of 90 m in the Union City, Oklahoma, tornado (Golden and Purcell 1978). To date, only a few in situ wind and pressure measurements are available in the vicinity of tornadoes (e.g., Fujita et al. 1970; Winn et al. 1999; Wurman and Samaras 2004; Lee et al. 2004). Recently, mobile Doppler

Corresponding author address: Dr. Wen-Chau Lee, Earth Observing Laboratory, NCAR, Boulder, CO 80303.
E-mail: wenchau@ucar.edu

radar measurements show that the peak wind in the most intense tornadoes exceeds 100 m s^{-1} (Wurman 2002, hereafter W02; Alexander and Wurman 2005, hereafter Part I; Wurman and Alexander 2005, hereafter Part II).

Doppler radar is the only current remote sensing instrument able to sample the three-dimensional internal structure of a tornado. The Doppler velocity is strictly an average of the particle motion within a radar pulse volume projected along a radar beam, weighted by the returned power from each particle. A radar integration volume is a function of radar pulse width, beamwidth (θ), and distance from the radar (r), and expands as the signal moves away from the radar. This volume also depends on the duration of the integration period used to calculate radar parameters and the antenna scan rate, resulting in blurred or larger effective volumes if integration times are long and/or scan rates are high. The maximum distance, r, from which a radar can resolve the tornadic vortex signature (TVS; Brown et al. 1978) is

$$r = \frac{D}{2\theta},$$

where θ is measured in radians, D is the distance across the TVS Doppler velocity dipole, and the constant in the denominator assumes a minimum of two radar samples across the TVS. From the sampling theorem (e.g., Carbone et al. 1985), it requires six–eight samples per wavelength to recover ~80% of the amplitude of a phenomenon. Therefore, the maximum distance for a radar to properly resolve a tornado circulation is 4 or more times closer than simply resolving a TVS. For a 1-km-wide tornado circulation (not the TVS) to be properly sampled by a 1° beamwidth Doppler radar, the radar has to be located within ~7 km of the tornado. Hence, it is not surprising that the National Weather Service's Weather Surveillance Radar-1988 Doppler (WSR-88D) network and other fixed ground-based Doppler radars infrequently capture the tornado circulation but almost exclusively sample the mesocyclone circulation (e.g., Brandes 1978, 1981; Burgess et al. 2002; Wurman and Alexander 2004). In addition, dual-Doppler analyses of nonsupercell tornadoes from fixed ground-based Doppler radars were presented in Wakimoto and Martner (1992) and Roberts and Wilson (1995). But their studies did not resolve the tornado core flow region because of limitations of data resolution outlined above.

Airborne Doppler radar such as the National Center for Atmospheric Research's (NCAR) Electra Doppler Radar (ELDORA) has sampled the tornadic region of supercells from 6 to 10 km away (e.g., Wakimoto et al. 1996). However, the 1.8° beamwidth of ELDORA and 300-m along-track resolution prevented accurate resolution of the core regions of tornadoes because of sampling limitations outlined above. The evolution of several mesocyclones embedded in these supercell storms has been resolved by ELDORA (Wakimoto et al. 1998; Wakimoto and Liu 1998; Wakimoto and Cai 2000; Dowell and Bluestein 2002a,b). The kinematic and thermodynamic structures retrieved from the dual-Doppler radar analyses are consistent with numerically simulated tornadic thunderstorms (e.g., Klemp and Rotunno 1983).

The development and deployment of the 3-cm-wavelength, mobile Doppler on Wheels (DOW; Wurman et al. 1997; Wurman 2001) and the mobile 3-mm-wavelength radar (Bluestein et al. 1995) in the mid-to-late 1990s provided new tools to sample tornadoes at very close range. Extreme wind speeds of tornadoes exceeding 100 m s^{-1} have been detected by mobile continuous wave (CW) and pulsed radars (Bluestein et al. 1993, 1997; Part I; Part II; W02). The DOWs and millimeter-wave radars have been deployed frequently within a few kilometers of tornadoes. These datasets with unprecedented resolution have revealed detailed reflectivity and velocity structures at the tornado scale (Wurman and Gill 2000, hereafter WG00; W02; Bluestein et al. 2003a,b; Part I; Part II). A downdraft along the central axis of a tornado indicating a partial two-cell vortex structure was also inferred from these data (WG00). However, the full tornado circulation can only be inferred from the data in these high-resolution single-Doppler radar datasets. Only recently, Wurman (1999), Richardson et al. (2001), and Dowell et al. (2002) resolved tornado circulations using dual-Doppler analyses on data collected from two DOWs. Bluestein et al. (2003a) resolved in two dimensions a weak tornado circulation using the ground-based velocity track display technique (GBVTD; Lee et al. 1999, hereafter LJCD) on one scan plane near the surface, and Dowell et al. (2005) calculated radial and tangential motions in a violent tornado.

Numerical models of varying complexity have been used to simulate aforementioned tornado structures and have offered insights in their dynamics (e.g., Snow 1978; Gall 1983; Rotunno 1977, 1979; Staley and Gall 1979, 1984). Tornado-like vortices have been successfully simulated in laboratory experiments (e.g., tornado vortex chamber; Ward 1972). In addition, theoretical limits on certain tornado elements such as the maximum wind speed, minimum pressure and thermodynamics of the downdraft, have been examined (e.g., Pauley et al. 1982; Snow and Pauley 1984; Snow et al. 1980; Fiedler and Rotunno 1986; Walko 1988). At-

tempts were made to measure these tornado characteristics in the tornado vortex simulator (e.g., Baker and Church 1979; Pauley 1989; Snow et al. 1980; Church and Snow 1985). Reviews of the above subjects can be found in Snow (1982), Davies-Jones (1986), Fiedler (1993), Rotunno (1986), and others. Recently, large eddy simulation of a tornado circulation at 10-m resolution has been presented in Lewellen et al. (1997) and Lewellen et al. (2000). Unfortunately, many of the kinematic and dynamic characteristics revealed in these studies have not been reproduced in observational studies, primarily because of the aforementioned limitations of Doppler radars.

The purpose of this paper is to demonstrate that the three-dimensional structure of a tornado can be deduced by applying the GBVTD techniques to high-resolution single-Doppler tornado data collected by a DOW and to examine a tornado's structure using this technique. This paper will focus on the axisymmetric aspects of the Mulhall, Oklahoma, tornado. It will be shown that the GBVTD-derived axisymmetric tornado circulation can be used to examine tornado dynamics simulated in the tornado vortex simulator and numerical models, but not previously revealed by observational data. Section 2 briefly reviews the data and methodology. Section 3 discusses the circulation centers of the Mulhall tornado. Section 4 presents the axisymmetric structure (tangential wind, radial wind, vorticity, perturbation pressure, and angular momentum). Section 5 presents the relationship between the swirl ratio and multiple vortices. A summary and conclusions are presented in section 6.

2. Data and methodology

The Mulhall tornado was one of several dozens of tornados that occurred over Oklahoma and Kansas on 3 May 1999. It was rated F4 on the Fujita scale (Speheger et al. 2002). The parent supercell [storm B by Speheger et al. (2002)], with a pronounced hook echo, was observed by the KTLX WSR-88D southeast of Oklahoma City, Oklahoma. This tornado was observed by a stationary and level DOW from 0310 to 0328 UTC 4 May 1999 (2210 to 2228 CDT 3 May 1999) from a deployment off Interstate 35, east of the town of Mulhall. The evolution and multiple-vortex structure of this tornado from the single-Doppler radar perspective has been documented in W02. The tornado was moving rapidly ($\sim$13 m s^{-1}) toward the north-northeast during this period. The tornado track from 0310 to 0323 UTC (hereafter, all times are UTC unless otherwise specified) and DOW deployment location are summarized in Fig. 1. Note that tornado translational motion, about 13 m s^{-1}, multiple-vortex perturbations up to 40 m s^{-1}, and inward/outward radial motions up to 15 m s^{-1} add or subtract from the axisymmetric tangential velocities to result in ground-relative velocities. Therefore, velocities to the east of the tornado, the location of the fatality on I-35 and in multiple vortices were likely substantially higher than indicated by the displayed radii. Localized Doppler velocities exceeded 109 m s^{-1} (W02). This tornado had an unusually large funnel cloud (see Fig. 6 in W02) and in fact is considered the largest documented tornado (Folkard 2005). The estimated radii of the near surface maximum wind and 40 m s^{-1} wind contours from the Doppler velocities were as large as 1.3 and 1.8 km, respectively (only 40 m s^{-1} radii shown in Fig. 1).

The DOWs have been deployed to sample high-resolution data in tornados and other small-scale and short-lived phenomena since 1995 (Wurman et al. 1997; Wurman 2001; W02; Part I; Part II). Characteristics of the DOWs can be found in Wurman (2001). For this deployment, scanning was conducted through azimuthal sectors of approximately 85°, at 12 stepped elevation angles of 0.3°, 1°, 2°, 3°, 4°, 5°, 7°, 9°, 11°, 13°, 15°, and 18°. Gate lengths were typically 25 m, and azimuthal oversampling resulted in data spacing of approximately 0.4°. The range of the tornado center from the DOW was 4–9 km, resulting in beam intersecting the tornado center between 30 and 1700 m above ground level (AGL; hereafter, all heights are AGL). Staggered pulse repetition frequencies were used to increase the Nyquist velocity to $\pm$128 m s^{-1}, nearly eliminating aliasing of Doppler velocities. Data spacing of 25 m $\times$ 32 m near the center of the tornado permitted features with scales as small as 100 m to be resolved reasonably (Carbone et al. 1985) and multiple vortices were evident in the return power and Doppler velocity fields (W02).

Fourteen 3D volumes of DOW data from 0310:03 to 0323:12 UTC were edited using NCAR's SOLO software (Oye et al. 1995) to remove noise, sidelobe contamination, rays with signal blockage near the surface, ground clutter, and other spurious data. Even with the $\pm$128 m s^{-1} Nyquist velocity, occasionally it was difficult to identify spurious data in the high shear region near the tornado core where gate-to-gate shear sometimes exceeded 1 s^{-1} [40 m s^{-1} (40 m)$^{-1}$]. These edited data were then interpolated onto a Cartesian grid using a bilinear interpolation algorithm. The translational motion of the tornado vortex was estimated by radar at 13 m s^{-1} toward 25° (consistent with the subjective result of 13.5 m s^{-1} in W02). Data were shifted in the grid using standard techniques to account for this translation. Then, the tornado centers were identified using the GBVTD-simplex algorithm outlined in Lee and

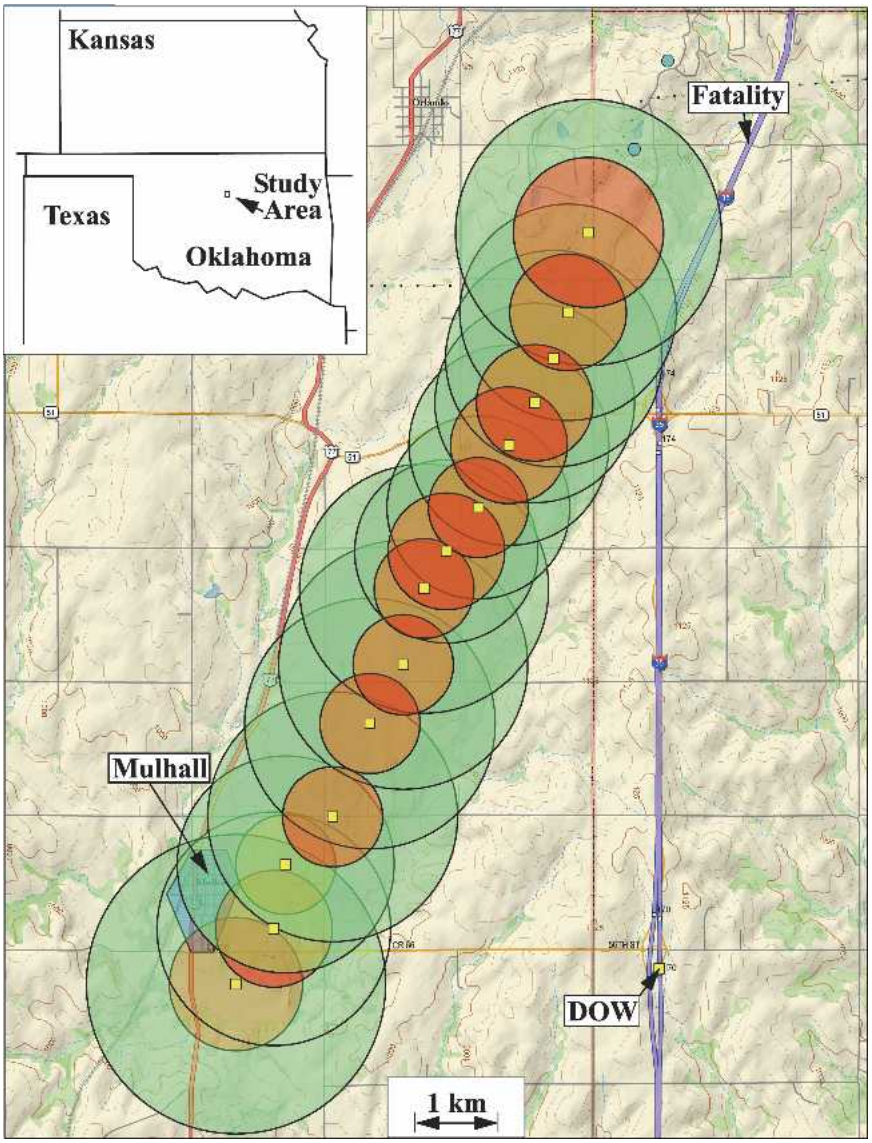

FIG. 1. Deployment location of DOW and tornado path. DOW location, tornado centers at 150 m AGL used in GBVTD algorithm, radii of maximum axisymmetric tangential wind (inner circles), and 40 m s^{-1} axisymmetric tangential velocity (outer circles) are shown. The gray polygon demarks the town of Mulhall, OK.

Marks (2000) at each altitude and time. Details will be discussed in section 3. Finally, the GBVTD analysis was performed to deduce the full axisymmetric tornado circulation.

The velocity track display (VTD) technique was originally proposed to extract the primary circulations of tropical cyclones from single airborne Doppler radar data on board the National Oceanic and Atmospheric Administration (NOAA) P3 aircraft (Lee et al. 1994). The VTD technique was formulated on a cylindrical coordinate system centered at the vortex circulation center. The VTD technique takes advantage of the near-circular nature of the primary (axisymmetric) vortex circulation and deduces the horizontal vortex circulation from the single-Doppler velocities. When using all available Doppler velocities along a constant radius, the tangential wind and radial wind of a vortex can be deduced via Fourier decomposition similar to the velocity azimuth display (VAD) technique (Browning and Wexler 1968). This formulation was modified in LJCD to be applied to tropical cyclone data collected by ground-based Doppler radars (e.g., WSR-88D) for a different scanning geometry and named as the GBVTD technique. In essence, the GBVTD is a more general

formulation and reduces to the VTD formulation when a radar is located at infinite distance from a tropical cyclone. LJCD discuss limitations of the GBVTD technique.[1]

The domain of the analyses extended from the center of the tornado to 3-km radius and from 50 to 1550 m in the vertical. Grid spacing in both the radial and vertical directions is 100 m, consistent with the radar sampling spacing. The quantities resolved in the GBVTD analysis include along-beam (connecting the radar and tornado center) component of the mean wind, axisymmetric tangential and radial winds, and the asymmetric tangential winds. Note that the unresolved asymmetric radial winds are aliased into the asymmetric tangential winds (LJCD). In this study, the truncated Fourier series was expanded up to wavenumber 10 anticipating the existence of multiple vortices within the Mulhall tornado (W02).

Once the azimuthally mean tangential and radial winds are obtained at each radius and height, the azimuthally mean divergence, vertical velocity, and angular momentum can be computed from the azimuthal mean (hereafter, mean represents azimuthal mean) tangential and radial winds following the methodology described in Lee et al. (2000). In addition, the mean vorticity in the cylindrical coordinates can be computed as follows:

$$\bar{\zeta} = \frac{1}{r}\left(\frac{\partial r\overline{V}_\theta}{\partial r} - \frac{\partial \overline{V}_R}{\partial \theta}\right). \tag{1}$$

Also, the full radial pressure equation excluding the Coriolis and friction terms

$$\rho\left(\underbrace{\overline{V_R}\frac{\partial \overline{V_R}}{\partial r} + \overline{w}\frac{\partial \overline{V_R}}{\partial z}}_{\text{Advection}} \underbrace{- \frac{\overline{V_\theta}^2}{r}}_{\text{Centrifugal}}\right) = \underbrace{-\frac{\partial p_a}{\partial r}}_{\substack{\text{Advection}\\ \text{pressure}}} \underbrace{-\frac{\partial p_c}{\partial r}}_{\substack{\text{Cyclostrophic}\\ \text{pressure}}} \tag{2}$$

can be evaluated. The pressure gradient term can be divided into advection pressure gradient, balanced with the advection terms (from the secondary circulation), and cyclostrophic pressure gradient, balanced with the centrifugal term (primary circulation). With the GBVTD-derived mean radial velocity ($\overline{V_R}$) and mean vertical velocity ($\overline{w}$), this is the first time that the advection pressure gradient of a tornado is estimated from Doppler radar observations.

3. Tornado center

In this paper, the tornado center is defined as a point that possesses the maximum mean vorticity at any given radius, that is, the maximum circulation enclosed by a circle. The radius that possesses the maximum GBVTD-derived mean vorticity is identified as the radius of maximum wind (RMW). According to the GBVTD formulation [Eq. (3) in LJCD], the axisymmetric circulation is relative to the mean wind (or environmental wind), which is a function of height. This is different from the commonly known storm-relative coordinate where the storm motion (a single vector, not varying with altitude) is traditionally computed from the observed differences in storm locations. In fact, the axisymmetric quantities of a vortex do not depend on the chosen coordinate systems. The circulation center is different from the wind center (zero wind speed) when there are nonzero environmental winds.

The initial tornado center of each volume is estimated from the return power and the zero Doppler velocity line. As described in Lee and Marks (2000), this initial center serves as a reference point to construct an array of 16 initial guesses for subsequent GBVTD-simplex algorithm and returns a total of 16 different center estimates. Ideally, these initial guesses of tornado centers should surround the true tornado center in all four quadrants to ensure that the consensus vorticity maximum is truly the global maximum. As a result, the scattering (standard deviation) of the resulting 16 GBVTD-simplex centers represents the level of confidence of the consensus tornado center (the arithmetic mean of the 16 answers). To filter out the outliers, centers that deviated more than one standard deviation away from the estimated tornado center were discarded. Then the new tornado center is the arithmetic mean of the remaining centers. These centers were further examined to ensure that the tornado structures (RMW and the maximum tangential wind) deduced from these centers were consistent in time at each altitude (Bell and Lee 2002).

The uncertainties of the tornado centers obtained from the GBVTD-simplex algorithm at each time and altitude are illustrated in Fig. 2. It is evident that the majority of the uncertainties are less than 20 m, comparable to the horizontal spacing of the radar data. Because of the radar scanning strategy, the area of missing data expands with increasing altitude. As a result, reliable centers above 1.2 km cannot be consistently obtained, indicated by larger standard deviations. Studies

[1] There is a typographical error in Eq. (20) of LJCD. The correct equation is $V_T C_0 = -B_1 - B_3 - V_M \sin(\theta_T - \theta_M)\sin\alpha_{\max} + V_R S_2$.

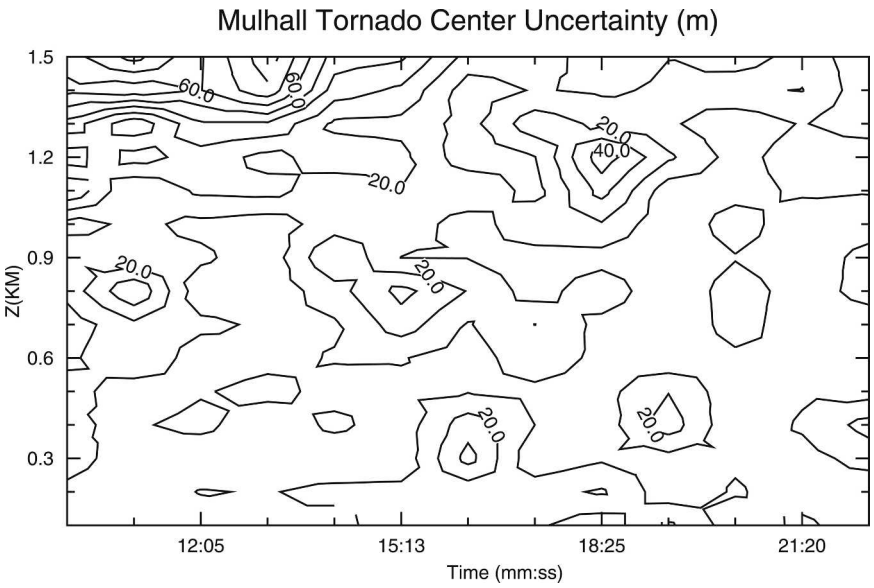

FIG. 2. The time–height distribution of the circulation center uncertainty estimated from the GBVTD-simplex vortex center algorithm (see text).

in Lee and Marks (2000) using idealized tropical cyclones recommended that the vortex centers need to be accurately determined within 5% of the RMW of the vortex in order to retrieve credible asymmetric structures (less than 1 km error of a 20-km RMW). The accuracy of the retrieved axisymmetric circulation (especially the tangential wind) is less sensitive to the uncertainty of the vortex center. The Mulhall tornado possessed an RMW of ~600 m. Therefore the center uncertainty needs to be less than 30 m in order to reliably retrieve the asymmetric circulation. Hence, the predominant 20-m uncertainty in tornado center presented here is not only adequate for the purpose of this study but also suitable for resolving asymmetric structures that will be the subject of future work.

Figure 3 illustrates the tornado track and vertical distribution of the centers for the 14 time periods. Note that the storm motion has been removed in the display of the vertical distribution of tornado centers. Starting with a 13.5 m s^{-1} toward 22.5° (all directions hereafter are in meteorological coordinates) translation speed, the final averaged storm motion, obtained from the centers at 50-m altitude, converged as 12.7 m s^{-1} toward 25.7° after several iterations of the procedure. The instantaneous tornado motion varied from 10 to 15 m s^{-1}. As a result, each volume of the data was shifted using its corresponding storm motion. The centers of the Mulhall tornado went through three cycles of vertical realignment during the observing period. In general, the tornado had a west–northwestward tilt in the lowest 1 km with the horizontal displacement ranging from ~400 to 500 m corresponding to a ~25° westward tilt from the vertical (e.g., 0311:09 UTC shown in Fig. 3b) to nearly upright (e.g., 0319:30 UTC shown in Fig. 3c). WG00 and Part I reported similar, 20°, tilts in the Dimmitt, Texas (1995), and Spencer, South Dakota (1998), tornadoes, respectively. Unfortunately, the Mulhall tornado occurred after dark, there was little available visual evidence corresponding to the above findings.

4. The Mulhall tornado

The axisymmetric structures of the Mulhall tornado will be presented using radius–height plots of the azimuthal mean quantities. It is understood that the tornado centers are tilted with height resembling a contorted tube. As a result, this form of presentation ignores the vertical tilt of the tornado. The axisymmetric structures of the tornado will be illustrated using the 0310:03 UTC volume as an example. The evolution of these structures and the tornado as a whole will be presented in the form of the time–distance plot (often referred to as Hovmöller diagram; e.g., Carbone et al. 2002).

a. The axisymmetric structure

The structure of the tornado at 0310:03 UTC is illustrated in Fig. 4. The tangential winds, illustrated in Fig. 4a (hereafter, all quantities are axisymmetric unless stated otherwise), increase from the calm tornado center to an annular peak wind of 79 m s^{-1} at $R = 700$ m and $z = 150$ m, then decrease beyond the RMW. The

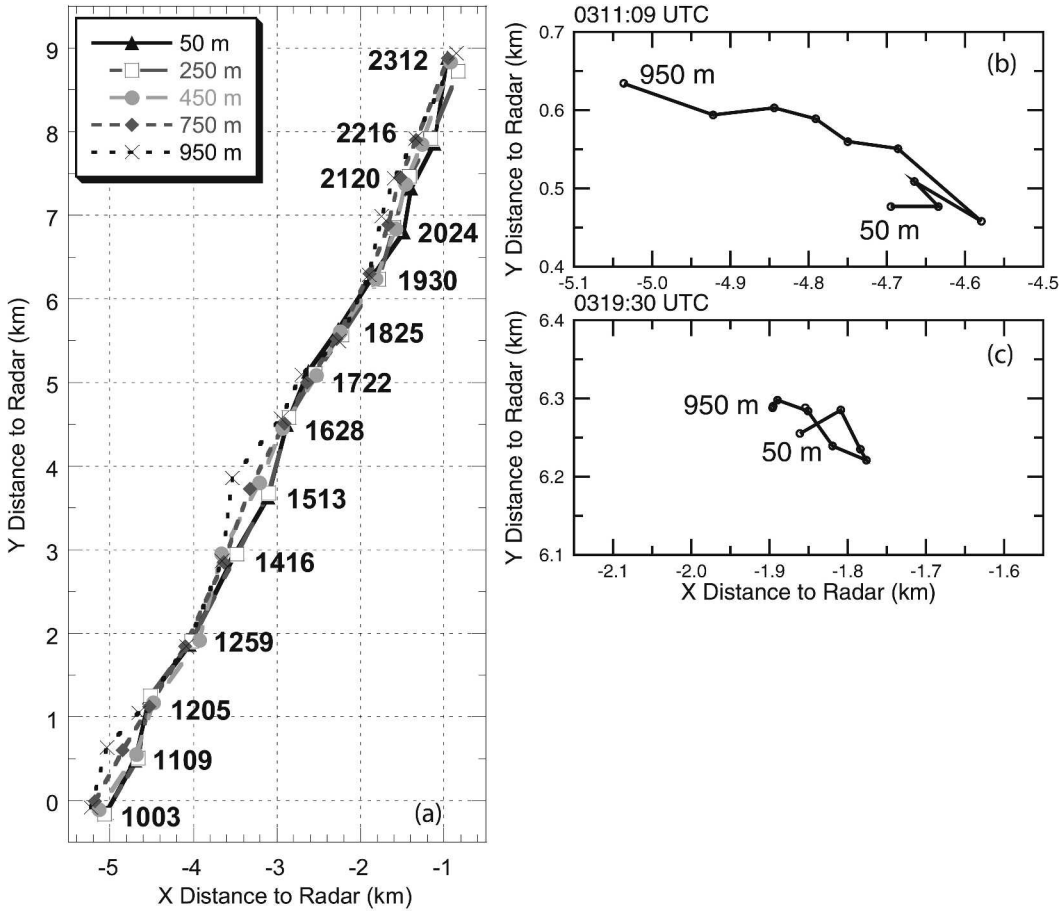

FIG. 3. (a) The circulation centers of the Mulhall tornado at five different heights during the observing period. The vertical alignment of the circulation centers oscillated between (b) a west-northwestward tilting mode, and (c) a nearly upright mode.

peak tangential winds decrease with height. The tangential wind profile resembles a miniature, intense tropical cyclone (about 1/15 in length scale) and possesses characteristics commonly seen in the inner core region of a mature tropical cyclone (e.g., Marks et al. 1992; Lee et al. 1994; Roux and Marks 1996; Lee et al. 2000). The radial profiles of the tangential winds at different altitudes versus a Rankine-combined wind profile corresponding to the winds at 50-m altitude are illustrated in Fig. 5a. The RMWs of the Mulhall tornado expand outward with height at ~16° from the vertical. From the normalized tangential wind profile (Fig. 5b), the winds on both sides of the RMW decrease less rapidly than the corresponding Rankine-combined vortex. The implication of this wind profile on vorticity and instability of this tornado will be discussed later in this section.

The secondary (meridional) circulation exhibits a classical two-cell circulation (Fig. 4b) commonly seen in tornado vortex chamber and numerical simulations under certain dynamical regimes (e.g., Ward 1972; Rotunno 1979). The downdraft inside the RMW turns into outflow and spreads outward at low levels (positive radial winds shown in solid lines), then collides with the inflow (negative radial winds shown in dashed lines) from the environment near the RMW and feeds into the annular updraft. Maximum convergence exceeding $-0.06\ s^{-1}$ is located inside the RMW (Fig. 4d), comparable to values of $-0.06\ s^{-1}$ found in the Spencer, South Dakota (1998), tornado (Part I). Outflow speed from the center peaks at 14 m s^{-1} and 50-m altitude. Peak inflow of 23 m s^{-1} is located at $z = 50$ m and 2.4-km radius. Since the lowest grid level is 50 m, this analysis suggests the peak inflow might occur below 50 m, as suggested by WG00 and Part I. The depth of the inflow layer reached 1 km but the most intense inflow was clearly confined near the surface. The average inflow depth is ~600 m for other times (not shown). The peak downdraft of 32 m s^{-1} is located at 400-m radius and 1350-m altitude near the top of the analysis domain.

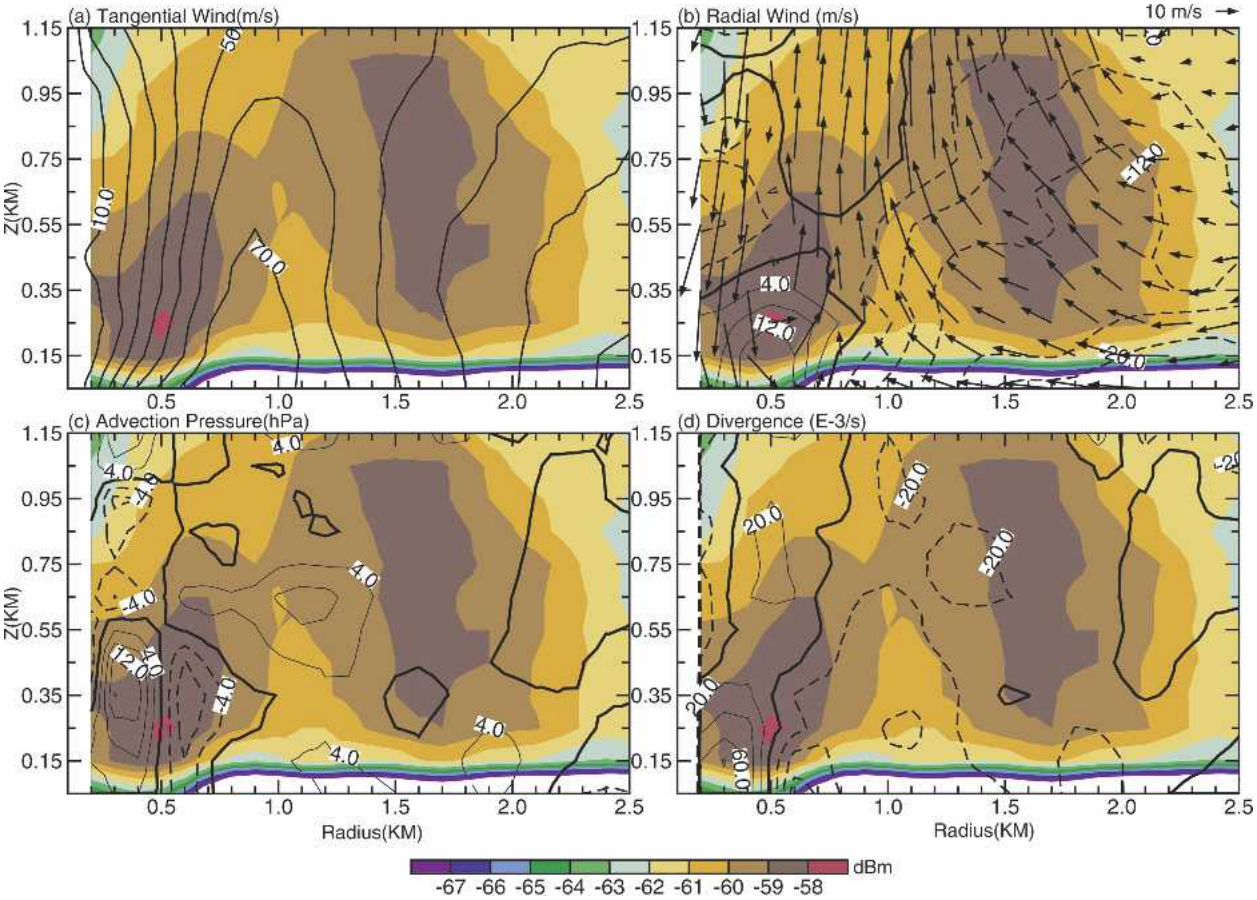

FIG. 4. The axisymmetric structure (radius–height) of the Mulhall tornado at 0310:03 UTC 4 May 1999. The return power is shown in grayscale and contours represent (a) tangential wind, (b) radial wind, (c) advection pressure deficit, (d) divergence, (e) cyclostrophic pressure deficit, (f) vorticity, (g) total pressure deficit, and (h) angular momentum. The vectors in (b) illustrate the secondary circulation of the Mulhall tornado. Solid (dash) lines represent positive (negative) values.

This intense downdraft is consistent with the divergence inside the RMW where it peaks (exceeding 0.08 s^{-1}) at $r = 300$ m and 150-m altitude. The downdraft magnitude of 30 m s^{-1} is comparable to the estimated downdraft speed reported in the Dimmitt tornado (WG00), which exhibited similar intensity.

Because Doppler radar measures primarily particle motion, not air motion, and this intense tornado likely contained significant debris, the GBVTD-derived radial winds have a positive bias owing to the centrifugal effect on the debris, which is proportional to the square of the tangential wind and inversely proportional to the radius (Dowell et al. 2005). Unfortunately, the exact bias at each grid point is unknown because of insufficient information on the type, size, and concentration of debris or precipitation particles. For a large raindrop, the estimated maximum bias of V_R near the RMW of 700 m and an 80 m s^{-1} tangential wind is on the order of 5 m s^{-1}. Therefore, the centrifugal effect would reduce (enhance) the inflow (outflow) magnitude and roughly shift the zero Doppler velocity line toward the tornado center by about 70 m at this time, resulting in the primary updraft being shifted closer to the tornado center as illustrated in Fig. 4a. This bias would result in a minor shift of the overall pattern but would not change the general results of this unusually large tornado presented in this study. The centrifugal effect ($\overline{V}_\theta^2/r$) decreases with increasing range outside the RMW because of a decrease in wind speed and an increase in radius. The centrifugal effect is also reduced inside the RMW (but at a slower rate) because of a faster reduction in the numerator compared with the denominator in the centrifugal term in Eq. (2). Nevertheless, these unknown biases should be small relative to the magnitude of the tornado circulation and should not affect the characteristics of the tornado presented in this study.

Figures 4c and 4e illustrate the retrieved perturbation pressure deficit from the advection and cyclostrophic

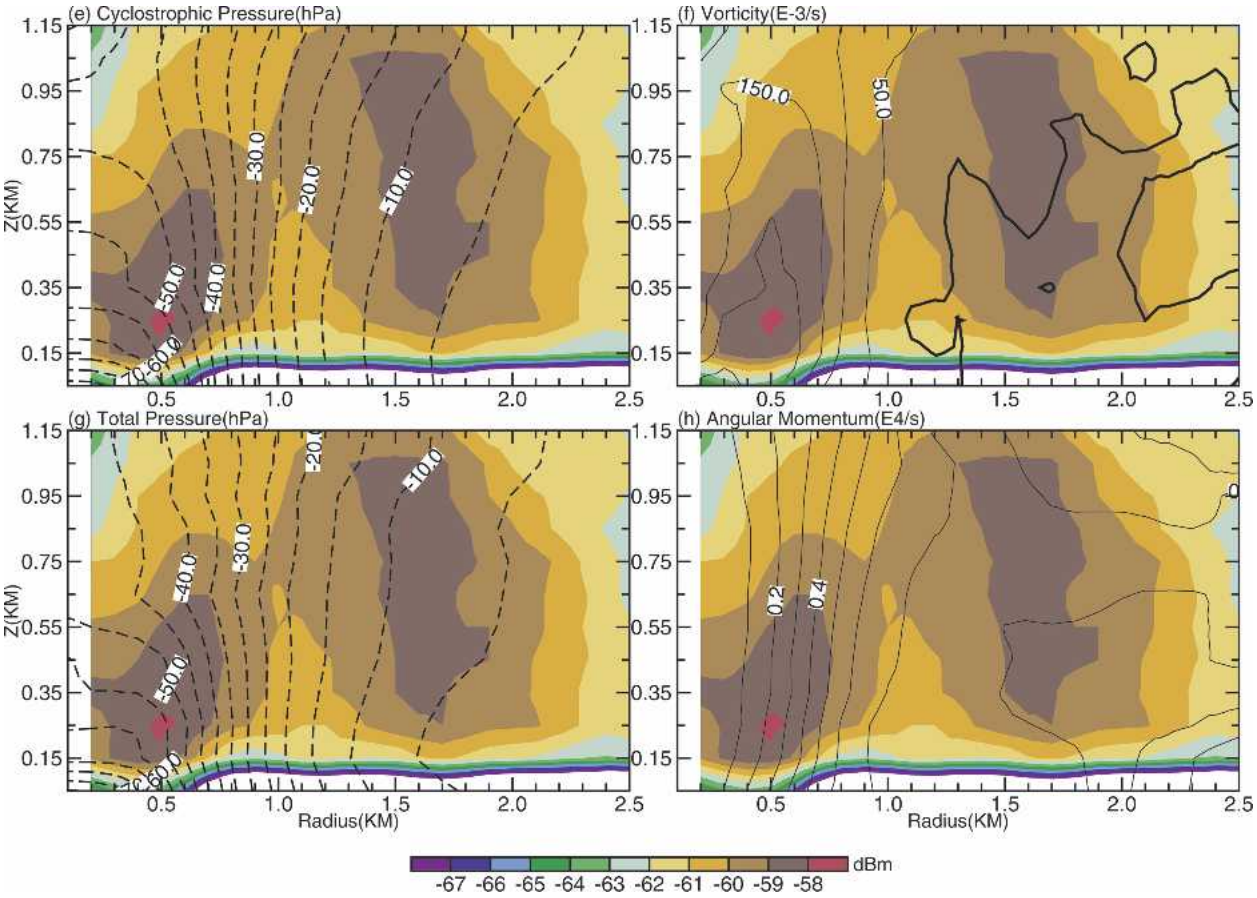

FIG. 4. (*Continued*)

terms in Eq. (2), respectively. The perturbation pressure deficit at each height is obtained independently assuming that the pressure perturbations at 3-km radius are zero at all heights. Therefore, interpretation of the vertical pressure gradient should be made with caution (e.g., Gal-Chen 1978). The cyclostrophic pressure (p_c) is in response to the swirling part of the tornado circulation, whereas the pressure from advection terms (p_a)

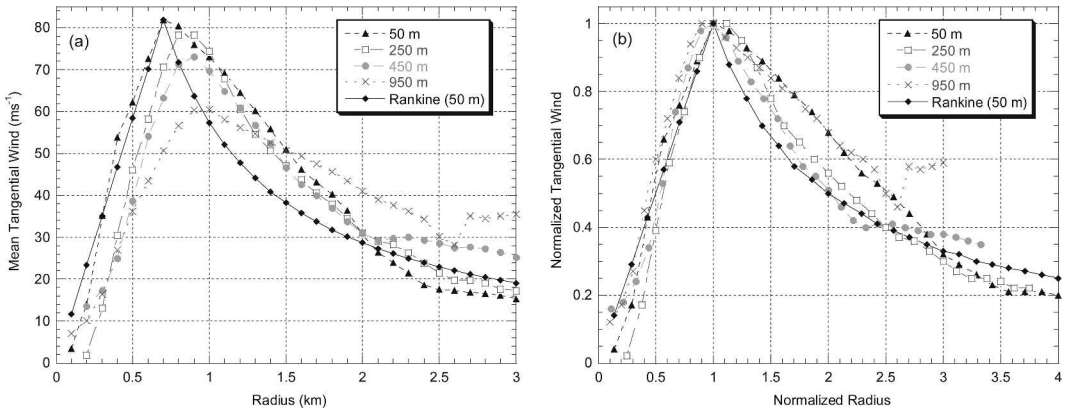

FIG. 5. (a) The radial profiles of the axisymmetric tangential wind of the Mulhall tornado at 0310:03 UTC 4 May 1999 at 50-, 250-, 450-, and 950-m altitude. (b) The aforementioned profile normalized to the peak tangential wind and RMW on each profile. Also shown is the Rankine-combined vortex constructed based on the normalized tangential wind profile at 50-m altitude.

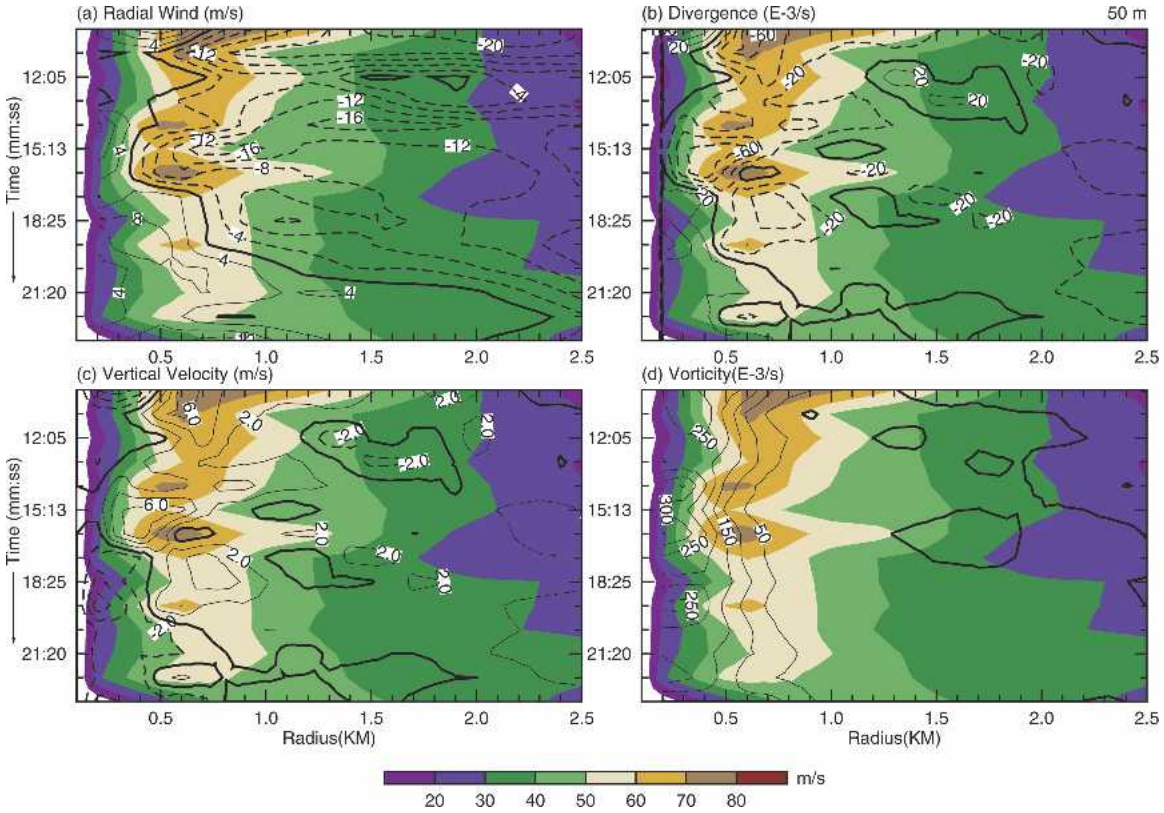

FIG. 6. Evolution of the Mulhall tornado at 50-m altitude presented in Hovmöller diagrams. The axisymmetric tangential wind is in grayscale. Contours are (a) radial wind, (b) divergence, (c) vertical velocity, and (d) vorticity. Solid (dash) contours represent positive (negative) values.

is in response to the secondary circulation, a component rarely, if ever, resolved in past observational studies of tornadoes.

The central cyclostrophic pressure (Fig. 4e) at $z = 50$ m is 81 hPa lower than the pressure at $r = 3$ km. About half of the pressure drop (~40 hPa) occurs near the RMW between $r = 500$ and 1000 m. The magnitude of the central pressure deficit decreases with altitude, consistent with the decrease of maximum tangential wind with height. The advection pressure perturbation (p_a) appeared to be an order of magnitude smaller than the cyclostrophic pressure perturbation (p_c) but the gradients of both, inside the RMW, were of the same order. The advection pressure gradient is consistent with the radial wind pattern of a two-cell circulation, specifically outflow from the center, inflow from the environment, and the decrease of the radial wind near the RMW. The deceleration of the central downdraft and the acceleration of the outflow at low levels are consistent with the high pressure (inside 500-m radius and below 500-m altitude) shown in Fig. 4c in a stationary state [Eq. (2)]. The total pressure (Fig. 4g) is dominated by the cyclostrophic pressure with adjustment in details from the advection pressure. For example, the total central pressure deficit is 3 hPa higher than the cyclostrophic central pressure deficit. These pressure deficits are comparable with rare in situ observations (Winn et al. 1999; Lee et al. 2004; Wurman and Samaras 2004) in strong tornadoes, as discussed in the next subsection. It can be shown that the central pressure deficit of a tornado possesses a variation of a Rankine-combined wind profile that can be derived analytically (details are provided in the appendix for interested readers). For a reasonable wind profile outside the RMW with a decay exponent $0.6 < b < 1.0$ and a $V_{\max} = 80$ m s^{-1}, the range of central deficit is between -91 hPa ($b = 0.6$) and 73 hPa ($b = 1$), which is consistent with the retrieved pressure deficit of -81 hPa.

The vorticity pattern in Fig. 4f shows an annular (or so-called ring) vorticity profile where the peak vorticity concentrated in an annulus $\sim r = 500$ m. The maximum cyclonic vorticity of 0.28 s^{-1} is located at $r = 300$ and 150 m altitude. The radial vorticity gradient of a ring vorticity profile changes sign and satisfies the necessary condition for barotropic instability, usually accompanying mature tropical cyclones (Mallen et al. 2005, here-

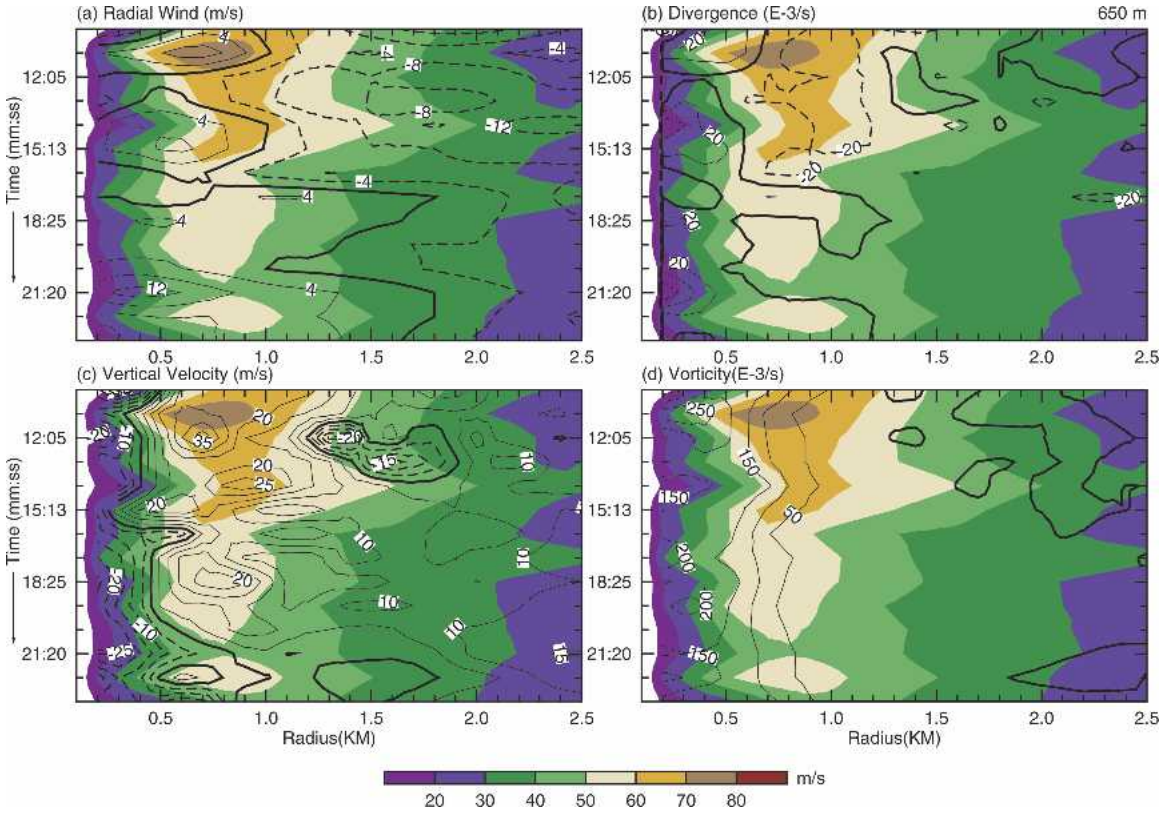

FIG. 7. Same as Fig. 6 but for 650-m altitude.

after M05). Near zero but weak negative vorticity (with a minimum of $-0.023\ s^{-1}$) was located outside RMW and below 600-m altitude. This vorticity profile is consistent with a non-Rankine vortex velocity profile shown in Fig. 5.

Figure 4h illustrates the angular momentum profile of this tornado. The angular momentum contours were nearly upright inside the RMW and their value increases with radius. The angular momentum outside the RMW increased at a slower rate and the contours were nearly horizontal below 250 m. This pattern is quite similar to those resolved within a mature tropical cyclone and suggests that the low-level inflow brings in higher angular momentum and the secondary circulation maintains the vortex (e.g., Lee et al. 2000; Marks et al. 1992; Rotunno and Emanuel 1987).

b. The evolution of the tornado

Even though the general axisymmetric characteristics of the tornado remain similar to that shown in Fig. 4, remarkable evolution was revealed during the 14-min observation period. The evolution is illustrated by Hovmöller diagrams of key parameters of the tornado at 50- and 650-m altitude shown in Figs. 6 and 7. As illustrated in Fig. 6a, the maximum mean tangential winds at 50-m altitude reintensified at 0314:16, 0316:28, and 0319:30 UTC but generally followed a decreasing trend from 79 to 49 $m\ s^{-1}$. This oscillation, with a period of 2–3 min, indicates that the ~1 min scan interval may still be inadequate to resolve the true evolution of this tornado. During this period, the RMW of the tornado shrank from 700 to 500 m then expanded to 1000 m. The peak maximum tangential wind of the entire event was 83 $m\ s^{-1}$ occurring at 0310:59 UTC and 450-m altitude (not shown). Peak observed Doppler velocities, not corrected for tornado motion, of near 110 $m\ s^{-1}$ were significantly higher, but were likely due to intense superimposed multiple vortices (W02).

The mean radial wind (contours in Fig. 6a) shows that the stagnation point (zero radial flow) was located at $r \sim 500$ m radius until 0314:16 UTC. The stagnation point contracted to $r \sim 300$ m at 0315:13 and 0316:28 then expanded beyond 2-km radius at 0323:12 UTC. The average depth of the inflow layer is ~600 m (not shown). There were three surges of low-level inflow at 0311:09, 0315:13, and 0318:25 UTC. The last two surges preceded the intensification of the tornado's tangential

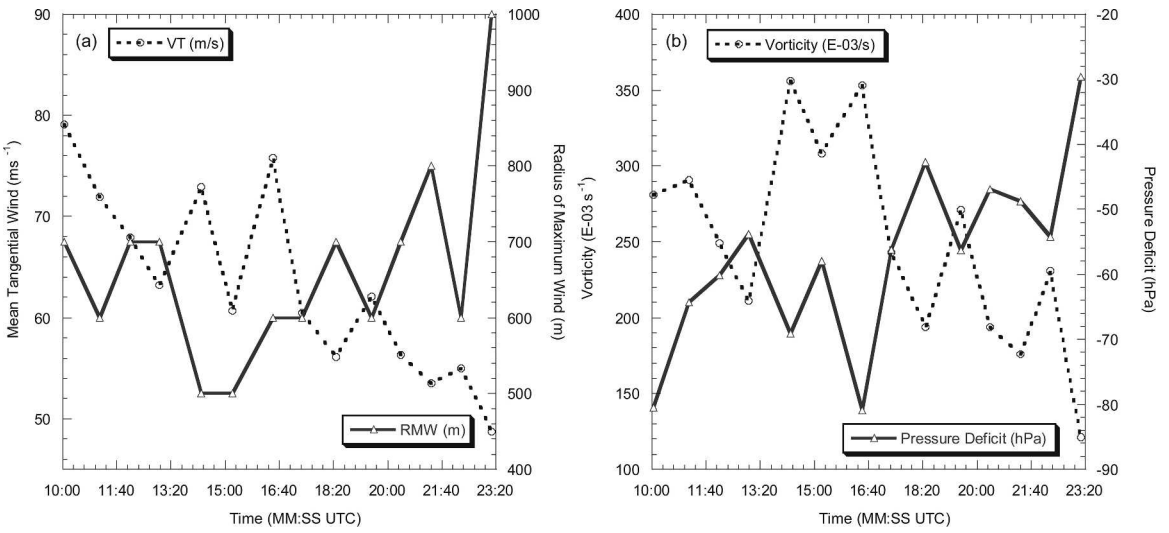

FIG. 8. Analysis of (a) the axisymmetric tangential wind vs RMW, and (b) the vorticity vs the total pressure deficit of the Mulhall tornado at 50-m altitude.

wind field at 0316:28 and 0319:30 UTC. At 150-m altitude, an inflow surge at 0312:05 UTC (not shown) preceded the intensification of the tangential wind at 0314:16. The oscillations of tangential winds and RMW are apparently out of phase, suggesting that vortex intensification is positively correlated with the shrinking of RMW (vortex constriction) during these episodes (Fig. 8a). The intensity oscillation at 650 m (Fig. 7a) is not as apparent as at 50 m but episodes of increased inflow can still be seen. Recall that the GBVTD-derived quantities were computed independently at each radius, altitude, and time. These coherent structures in space and time suggest that the reintensification of the tornado is a physically plausible event, not an artifact of the analysis.

The divergence at 50 m (Fig. 6b) is positive (negative) inside (outside) the RMW with peak convergence of 0.08 s^{-1} at 0315:13 UTC while the magnitude is much smaller at 650 m (Fig. 7b). This is consistent with the downdraft (Fig. 6c) inside the RMW penetrating to 50 m altitude at all times except at 0315:13 UTC (when it reached to only 150 m, Fig. 9a), implying that the tornado maintained a two-cell structure throughout the observing period. This is in contrast to the two-cell structure inferred in the Dimmitt, Texas (1995), tornado (WG00), in which the downdraft did not reach near the ground. The updraft constricted and intensified (Fig. 7c) before the vortex intensification at 0314:16, 0316:28, and 0319:30 UTC, consistent with the displacement of the stagnation point. A second updraft core (>10 m s^{-1}) formed beyond 2 km after 0312:59 (Fig. 7c). After 0320:24 UTC, the inner updraft dissipated and the outer updraft became the primary updraft (Fig. 7c). The primary and secondary circulations of the tornado at 0316:28, 0320:24, and 0323:12 UTC (Fig. 9) clearly illustrate the intensifying (weakening) of the outer (inner) updraft associated with the outward shift of the region of most intense debris and/or rain as manifested by the maximum in return power. Interestingly, a separate tangential wind maximum at outer radii was not developed in association with the intensification (diminishing) of the outer (inner) updraft, as is commonly associated with the eyewall replacement cycle observed in mature tropical cyclones (e.g., Willoughby et al. 1982). At 0323:12 UTC, the RMW expanded to 1000-m radius compared with the peak updraft located beyond 2-km radius. The reasons for this decoupling are not known. The most intense updraft (41 m s^{-1}) occurred earlier in the period at 1.15-km altitude and 700-m radius at 0312:05 UTC (not shown). The most intense downdraft (47 m s^{-1}) occurred twice at 200-m radius and 1.15-km altitude (not shown). The first instance was 0315:13 just before the reintensification at 0316:28 and the second at 0321:20 UTC when the inner updraft dissipated.

The perturbation pressure pattern at the tornado center is directly correlated with the location and magnitude of the maximum tangential wind at each height as shown in the appendix. When the analysis domain (r_2) is greater than 4–5 times of the RMW, the computed pressure deficit is within a few hectopascals of the true pressure deficit as the pressure curves flatten out (Fig. A1). In addition, the pressure deficit is mainly dependent on the maximum tangential wind and nearly independent on the RMW (i.e., size of the tornado). The pressure gradient was concentrated near the RMW

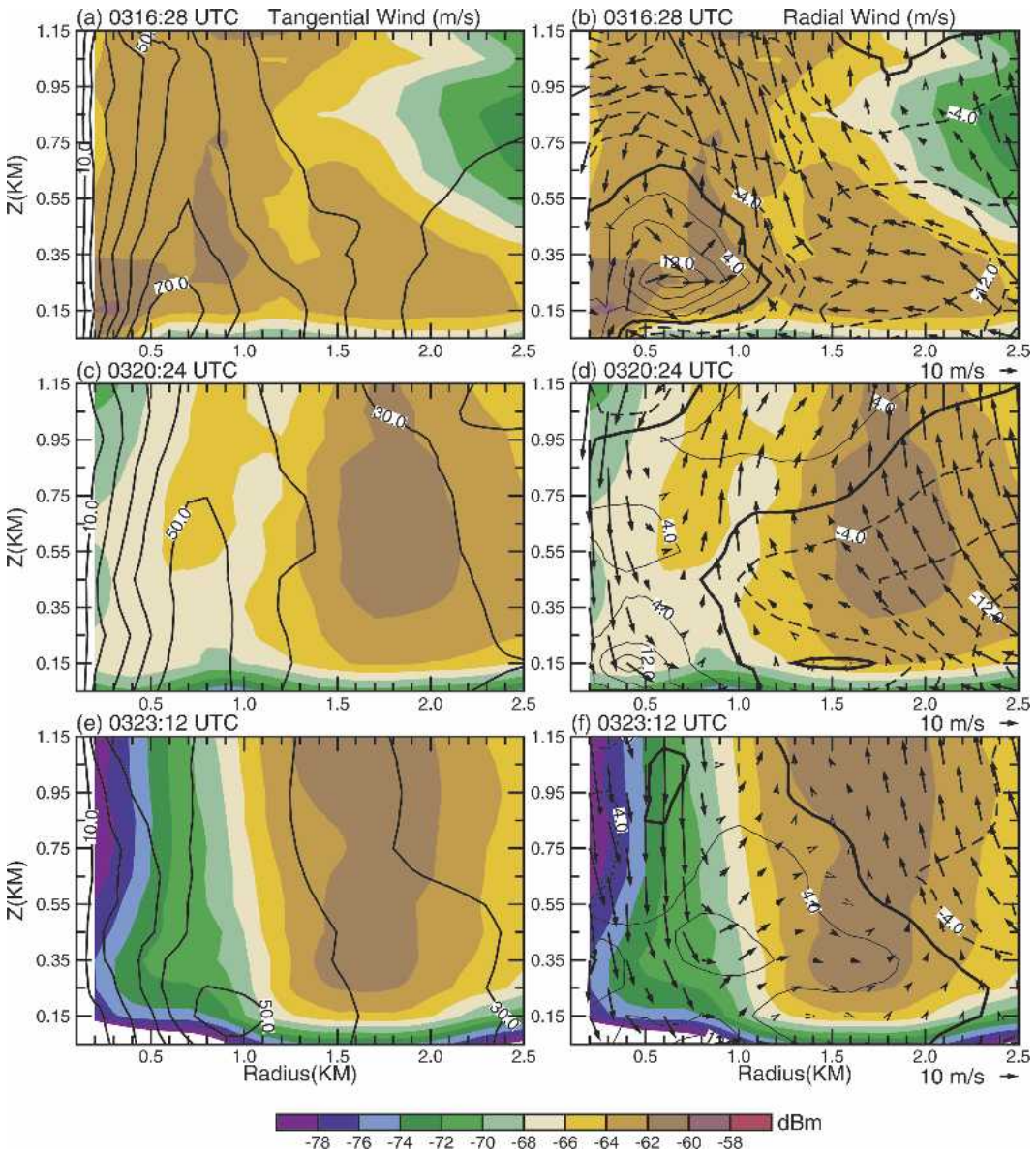

FIG. 9. The (left) primary and (right) secondary circulations of the Mulhall tornado at (a), (b) 0316:28, (c), (d) 0320:24, and (e), (f) 0323:12 UTC. Return power is represented in grayscale. Positive (negative) values are in solid (dash) lines.

and was more intense at low levels. The lowest perturbation pressure of −84 hPa occurred at 0310:59 UTC at 450-m altitude (consistent with the peak tangential wind of 83 m s^{-1}, not shown). The perturbation pressure deficit at 50 m altitude reached −80 hPa at 0310:03 and 0316:28 UTC (Fig. 10). After that, the perturbation pressure fluctuated between −40 and −50 hPa.

In situ pressure measurements in tornadoes are rare. The first surface pressure measurement of a large tornado is the E-Turtle pressure trace of the F4 Allison, Texas, tornado in 1995 (Winn et al. 1999). Although there is only limited Doppler radar data to confirm the size of the Allison tornado (Wurman and Alexander 2004), a 1.3-km-wide F3 damage swath indicated that it might have been unusually large and similar in size to the Mulhall tornado. Figure 10 shows the comparison among perturbation pressure profiles at four times (0310:03, 0312:59, 0316:28, and 0319:30 UTC) of the Mulhall tornado derived from the GBVTD technique and the Allison tornado measured by an E-Turtle (all pressure deficits are normalized at r = 3 km). Note that Winn et al. (1999) estimated that the particular

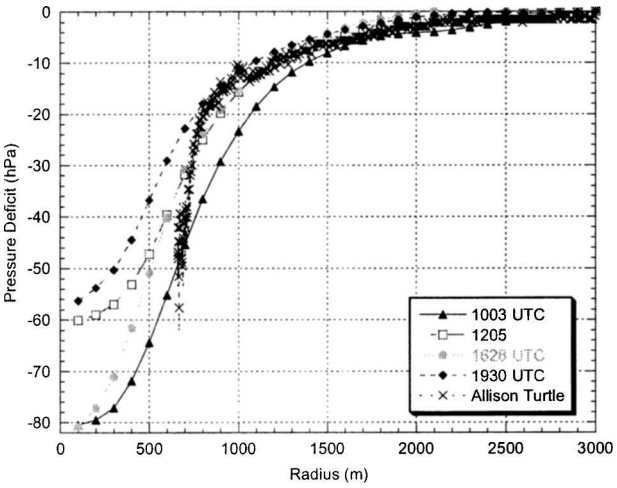

FIG. 10. The total pressure deficits (normalized at 3-km radius) of the Mulhall tornado retrieved from the GBVTD-derived tangential wind at 50-m altitude and four different times (0310:03, 0312:59, 0316:28, and 0319:30 UTC). Also shown is the pressure deficit of the Allison tornado (1995) measured by an E-Turtle during VORTEX-95. The location of the E-Turtle was estimated as close as 600 m from the F4 Allison tornado.

E-Turtle was located as close as 660 m from the tornado center. These pressure profiles show remarkable similarity between $r = 800$ m and 3 km except for the 0310:03 UTC. The pressure drop off in the Allison tornado appeared much sharper inside $r = 800$ m while the retrieved pressure drop in the Mulhall tornado was smoother. This may be attributed to the differences in intrinsic storm structures and/or the sampling methods. The E-turtle measured a pressure trace of a particular path through the tornado in contrast to the axisymmetric pressure retrieved in this study. Wurman and Samaras (2004) illustrates how a suction vortex can sharpen the local pressure pattern similar to the incomplete pressure records shown in Fig. 10. Nevertheless, the magnitudes of the total pressure deficit were quite comparable in both tornadoes.

More recently, in situ pressure measurements have been obtained in two tornadoes (Wurman and Samaras 2004; Lee et al. 2004). A pressure deficit of 41 hPa was observed in tornado north of Stratford, Texas (2003), containing peak DOW-measured winds of 53 m s^{-1}, and DOW measured RMW of 200 m. Peak cyclostrophic winds, calculated from the pressure data, were 45 m s^{-1}. A pressure deficit of 100 mb was measured in the Manchester, South Dakota (2003), tornado that caused F4 intensity damage shortly prior to the in situ observation. Peak cyclostrophic winds, calculated from the pressure data, were near 80 m s^{-1}. These recent observations have not been sufficiently analyzed to permit detailed comparison with the pressure deficit profiles presented herein. However, the qualitative agreement in the central pressure deficits measured in these tornadoes and the results presented herein are encouraging.

Intense axisymmetric vorticity was concentrated at low levels. Peak vorticity at 50-m altitude was 0.36 s^{-1} and occurred at 0314:16 and 0316:28 UTC. The negative correlation between the vorticity (also tangential wind) and the pressure deficit is quite clear (Fig. 8b). Although the tangential wind at 0310:03 UTC is greater than during those aforementioned periods, a larger RMW at that time results in a weaker vorticity. From 0310:03 to 0319:30 UTC, the vorticity field possessed a maximum at $r \sim 400$ m (ring vorticity pattern, cf. Fig. 6d). After 0320:24, the vorticity peaked at the tornado center and monotonically decreased outward. Based on a composite study of near-core vorticity distribution using 23 yr (1977–99) of hurricane reconnaissance data, the ring vorticity pattern is associated with major hurricanes while the monotonically decreasing vorticity pattern is associated with pre-hurricane storms and minimal hurricanes (M05). The relationship between the vortex intensity and its corresponding vorticity pattern presented in this study are consistent with that within tropical cyclones. However, similarity in kinematic structures does not imply that tornadoes and hurricanes are dynamically similar, an interesting subject for future study. The ring vorticity pattern also satisfies the necessary condition of barotropic instability where radial vorticity gradient changes sign in the domain (Holton 1979, p. 354).

5. Swirl ratio and multiple vortices

During the majority of the observation period, the Mulhall tornado's vorticity profile satisfied the necessary condition of barotropic instability. This suggests that perturbations may grow on the parent axisymmetric vortex. Tornado-like vortices have been successfully simulated in a tornado vortex chamber (Ward 1972; Church et al. 1979) and numerical simulations (e.g., Rotunno 1977, 1979). Both type of studies suggested that the single most important nondimensional parameter that governs the tornado-like vortex structure/dynamics is the swirl ratio (S), the ratio between the rotational wind and the mean vertical velocity within a tornado. One form of the swirl ratio is defined as

$$S = \frac{1}{4}\frac{2R}{h}\frac{v_R}{u_R}, \tag{3}$$

where R, h, v_R, and u_R are the updraft radius, inflow

depth, and tangential and radial winds at radius R (Rotunno 1979), respectively. The relationship between the swirl ratio and tornado structure is summarized in Fig. 11 (Davies-Jones 1986).

The parameters used to compute swirl ratio in Eq. (3), such as the updraft width and inflow depth are specific for a given tornado vortex chamber and tornado simulations in the aforementioned simple axisymmetric numerical models while the vertical and horizontal mass flux are controlled quantities. In the GBVTD-derived axisymmetric structures of the Mulhall tornado, however, these parameters are not clearly (uniformly) defined. For example, R and h are determined as the radius at the edge of the updraft and the average depth of the inflow layer while u_R and v_R are defined as the mean inflow speed and the tangential wind speed at the edge of the updraft. The purpose of this computation is to examine the qualitative relationship between regimes of the tornado flow structure and S. Although the swirl ratio of a tornadic storm has been computed using dual-Doppler winds (Wakimoto et al. 1998), this study presents the first swirl ratio computation in a resolved tornado circulation using single-Doppler radar-retrieved tornado winds.

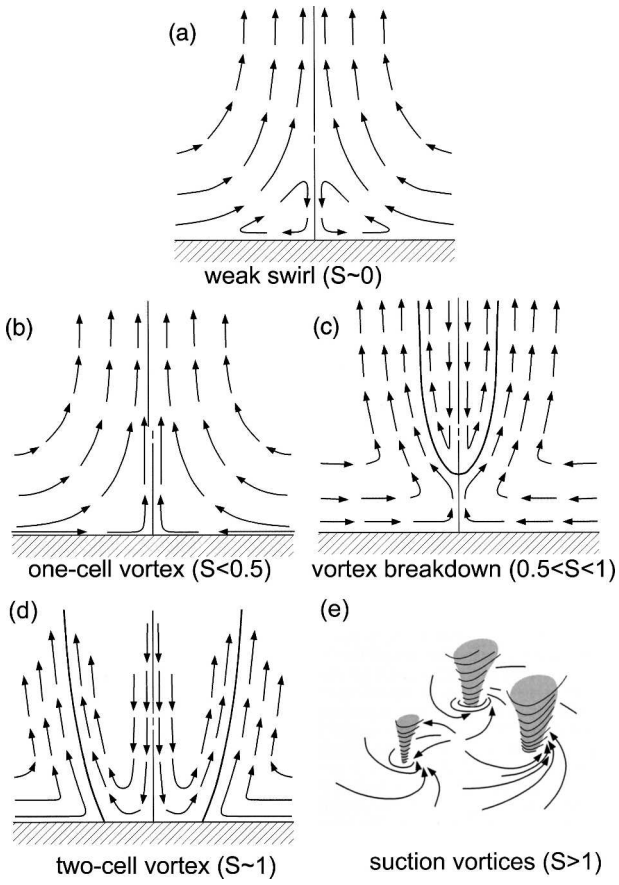

FIG. 11. Schematic diagrams of tornado-like vortex structures as a function of swirl ratio. (Adapted from Davies-Jones 1986.)

The swirl ratios of this tornado and the corresponding kinematic parameters in Eq. (3) are listed in Table 1. The swirl ratios during the entire observational period (~14 min) are all above 2 (clearly much greater than 1). Therefore, the uncertainties in S, possibly resulting in errors of as much as a factor of two, owing to subjectively choosing representative values of these parameters should not affect the general conclusions. When $S > 1$, according to the tornado vortex chamber and numerical simulation results (as illustrated in Fig. 11), the tornado should possess a two-cell structure as was clearly deduced in all 14 volumes of the GBVTD analyses. Another distinct property within a simulated tornado with a swirl ratio greater than 1, is the presence of multiple vortices. This is also consistent with the observed return power and single-Doppler velocity structures where small-scale rings in return power accompanied by Doppler velocity couplets can be identified throughout the observation period (W02). Signatures of the multiple vortices can be clearly identified between 0314:16 and 0317:22 UTC. A striking example is illustrated in Fig. 12 where six small vortices can be identified on the west side of the tornado, especially in the velocity field, at 1316:28 UTC. The GBVTD-derived tangential wind (when fitting the Fourier series to wavenumber 10) at 1316:28 UTC (Fig. 13) clearly shows the nature of multiple vortices near the RMW and higher winds on the west side of the tornado where multiple vortices resided. However, the GBVTD analysis did not resolve meaningful amplitudes beyond wavenumber 4 so the apparent higher wavenumber multiple vortex structure shown in Fig. 12 was likely aliased on

TABLE 1. Swirl ratios (S) of the Mulhall tornado from 0310:03 to 0323:12 UTC and its subjectively chosen parameters in Eq. (3).

UTC	R (km)	h (km)	u_r (m s^{-1})	v_r (m s^{-1})	S
0310:03	2	1.0	16	35	2
0310:57	1.5	0.5	16	40	4
0312:05	1.5	0.6	15	40	3
0312:59	1.5	0.5	10	40	6
0314:16	2.0	0.8	12	40	4
0315:13	2.5	0.6	16	30	4
0316:28	1.5	0.6	16	40	3
0317:22	1.5	0.6	8	32	5
0318:25	2.5	0.8	16	25	2
0319:18	2.8	0.7	20	20	2
0320:24	3.0	0.7	20	25	3
0321:20	3.0	1.0	18	25	2
0322:16	3.0	1.0	10	20	3
0323:12	3.0	1.0	12	20	3

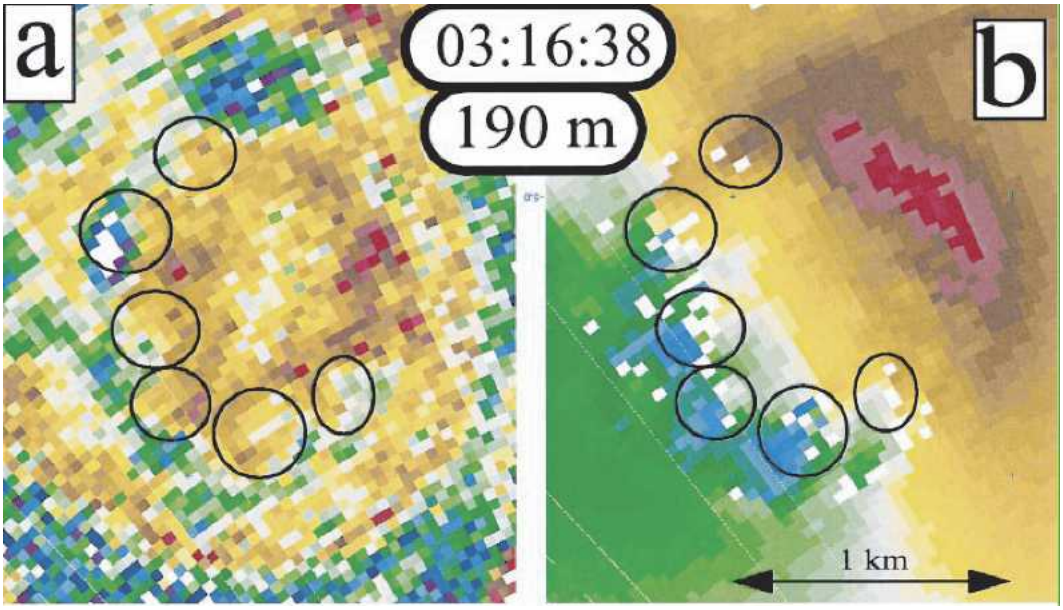

FIG. 12. (a) Power and (b) Doppler velocity fields in the tornado illustrating a train of quasi-periodic multiple vortices with high wavenumber. The black ellipses mark at least six multiple vortices in the tornado at 0316:28 UTC and 190-m altitude.

to lower wavenumbers in the GBVTD analysis (Fig. 13) probably because of insufficient angular resolution of these small vortices in the DOW data. Note that the swirl ratios in the first half of the observation period are generally larger (approximately twice as large) than those in the latter half of the period. The maximum swirl ratio reaches 6 at 1312:59 UTC and a second maximum of 5 at 1317:22 UTC. The qualitative agreement between the tornado's reflectivity and velocity structure and the derived swirl ratio further show the GBVTD-derived tornado structures are physically plausible.

6. Summary and conclusions

This paper has presented, for the first time, physically consistent 3D axisymmetric structures of a tornado deduced from a mobile Doppler radar and the GBVTD technique. The GBVTD-derived axisymmetric kinematic quantities were used to compute several dynamic parameters of the tornado. This study confirms a number of kinematic and dynamic aspects of a tornado only previously simulated in tornado vortex chamber and axisymmetric numerical models for over 20 years, including the two-cell circulation, the angular momentum profile, the pressure pattern, the relationship between swirl ratio and multiple vortices, and the correlation between vortex intensity and the vorticity profile. Ma-

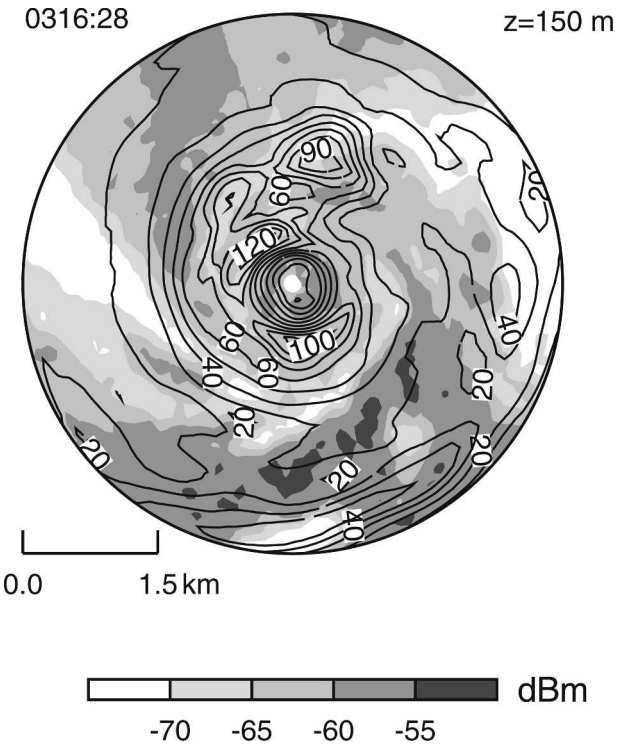

FIG. 13. The GBVTD-derived tangential wind (contours, unit in m s^{-1}) of the Mulhall tornado at 0316:28 UTC and 150-m altitude. Return power is in grayscale.

jor characteristics of the Mulhall tornado include the following:

1) The tornado center tilted west–northwestward with height and oscillated between nearly vertical to an angle as large as 25° over the lowest 1.5 km.
2) A two-cell circulation was revealed by the GBVTD analysis, similar to those often observed in mature tropical cyclones.
3) The axisymmetric low-level inflow had an average depth ~600 m but intense inflow occurred near the surface. The inflow layer was much deeper than the shallow inflow in the corner flow region. The deep inflow layer may be unique to large tornadoes.
4) The tornado intensity (maximum mean tangential wind) oscillated with a several-minute period. The increase (decrease) of intensity correlates well with decrease (increase) of the RMW and was preceded by surges of the low-level inflow.
5) The primary updraft was first collocated with the RMW but was replaced by an outer annulus of updraft (beyond 2-km radius) during the decaying stage of the tornado. This process resembles the eyewall replacement process in a mature tropical cyclone. However, the outer wind maximum did not develop in this case.
6) The maximum central pressure deficit at 50-m altitude from 3-km radius to the tornado center was approximately 80 hPa, in good agreement with the in situ measured pressure deficit in the similar-strength Allison, Texas (1995), and Manchester, South Dakota (2003), tornadoes. The magnitude of the central pressure deficit was consistent with the pressure deficits computed from the cyclostrophic equation using analytical, modified Rankine-combined wind profiles. These may be typical pressure deficits associated with large and/or violent tornadoes.
7) During the most intense stage of the tornado, the vorticity possessed a ring pattern that satisfied the necessary condition of barotropic instability. The weakening of the tornado was associated with a monotonically decreasing vorticity profile. Both of the intensity–vorticity relationships are consistent with those observed in tropical cyclones and theoretical studies. The similarity of the axisymmetric kinematic and vorticity characteristics between this tornado and mature tropical cyclones are striking. Unfortunately, the lack of thermodynamic measurements within tornadoes prevents further comparison of the forcing mechanisms and energy sources between these two types of atmospheric vortices.
8) The computed swirl ratios are between 2 and 6, consistent with the unstable vorticity profiles and the observed multiple vortex structures of the tornado.

The ability to deduce the 3D tornado structures from single-Doppler observations expands the usable tornado datasets beyond the limitations imposed by traditional dual-Doppler analyses. Although the results presented in this study are valid for one case, it is natural to extend the methodology to other tornadoes of different sizes and intensities in order to examine whether tornadoes in nature behave like those simulated in the laboratory and numerical models. This study also exposes the need to have the volume scan time shorter than one minute to properly resolve the rapid evolution of tornadoes. This capability has recently become available through a new rapid-scanning DOW (Wurman and Randall 2001).

Acknowledgments. The authors would like to thank Michael Bell for processing DOW data and generating figures for this manuscript and Renee Ray for assistance with the manuscript. The authors are grateful for the suggestions provided by Drs. R. Rotunno, J. Wilson, N. Dotzek, and two anonymous reviewers. Their comments and suggestions greatly improved the quality and presentation of this paper. This research is partially supported by the National Science Foundation CAREER Grants NSF-ATM-9703032 and NSF-ATM-0437505. Herb Stein and William Martin and one of us (Wurman) operated the DOW during a challenging nighttime tornado intercept. The DOW radars are operated by the Center for Severe Weather Research with close collaborations with the National Center for Atmospheric Research.

APPENDIX

Analytical Derivation of Central Pressure Deficit in Tornadoes

Assuming cyclostrophic wind balance within a tornado (e.g., Lewellen 1976), the balance between tangential velocity and pressure in a circular vortex can be written as

$$\frac{dp'}{dr} = \rho(p)\left[\frac{v^2}{r}\right], \tag{A1}$$

where p', r, v, f, ρ are pressure, radius, axisymmetric and tangential velocity, and density, respectively. In this derivation, the density is assumed constant at each altitude; therefore, it is independent of p.

If one knows $v(r)$, one can compute the pressure dp'/dr as a function of r; then integrate Eq. (A1) from a finite radius to the tornado center to obtain the pressure deficit (Δp) at the center of the tornado. The purpose of this appendix is to illustrate that Δp can be estimated analytically for tornadoes in which the wind profiles resemble a modified Rankine combined vortex as follows:

$$V = V_{\max}(r/\mathrm{RMW}) \quad \text{when} \quad r < \mathrm{RMW}, \tag{A2}$$

$$V = V_{\max}(\mathrm{RMW}/r)^b \quad \text{when} \quad r > \mathrm{RMW}, \tag{A3}$$

where RMW is the radius of maximum axisymmetric tangential wind and b is the decay exponent of the tangential wind outside the RMW.

When substituting Eqs. (A2) and (A3) into (A1) and integrating (A1) from $r = r_2$ *to* $r = 0$, one obtains

$$\begin{aligned}\frac{1}{\rho}\Delta p &= \int_{\mathrm{RMW}}^{0} \frac{V_{\max}^2(r/\mathrm{RMW})^2}{r}\,dr + \int_{r_2}^{\mathrm{RMW}} \frac{V_{\max}^2(\mathrm{RMW}/r)^{2b}}{r}\,dr = \frac{1}{2}V_{\max}^2\left(\frac{r}{\mathrm{RMW}}\right)^2\Bigg|_{\mathrm{RMW}}^{0} + \frac{(\mathrm{RMW}^b V_{\max})^2}{-2b}\,r^{-2b}\Bigg|_{r_2}^{\mathrm{RMW}} \\ &= \left[0 - \frac{1}{2}V_{\max}^2\right] - \left[\frac{(\mathrm{RMW}^b V_{\max})^2}{2b}\,\mathrm{RMW}^{-2b} - \frac{(\mathrm{RMW}^b V_{\max})^2}{2b}\,r_2^{-2b}\right] \\ &= -\frac{1}{2}V_{\max}^2 + \frac{(\mathrm{RMW}^b V_{\max})^2}{2b}(r_2^{-2b} - \mathrm{RMW}^{-2b}) = -\frac{1}{2}V_{\max}^2 + \frac{V_{\max}^2}{2b}\left[\left(\frac{\mathrm{RMW}}{r_2}\right)^{2b} - 1\right].\end{aligned} \tag{A4}$$

Equation (A4) states that the calculated total pressure drop of an atmospheric vortex measured from a point $r_2 >$ RMW is due to the contribution from the solid body rotation region $r <$ RMW (first term) and the exponential decay region $r >$ RMW (second term). If $r_2 <$ RMW, in the case where the pressure drop at the center is calculated relative to a point inside RMW, then only part of the drop due to the solid body portion of Eq. (A4) is realized. In the usual case of $r_2 >$ RMW, the total pressure drop depends on four parameters, $V_{\max}$, RMW, the outermost radius of available wind information (r_2), and the exponent of the decay of the wind profile outside of RMW (b). Note that when r_2 approaches infinity, Δp is a function of $V_{\max}$ and b (i.e., the size of the tornado is irrelevant in computing the central pressure deficit). Assuming the average density $\rho = 1.17$ kg m^{-3} at 950 hPa at the surface and $r_2 =$ 5 RMW, the central pressure deficits (Δp) for a variety of wind profiles can be computed (Table A1).

The sensitivity to the choice of r_2 is illustrated in Fig. A1. It can be seen that for $0.6 < b < 1.0$, the pressure curves flatten out after $r_2 = 5$RMW, and that the potential error is only several hPa. The calculated pressure deficit for a tornado with $V_{\max} = 80$ m s^{-1} and $b =$ 0.6–0.7, similar to the Mulhall tornado, is 85 to 91 hPa, very similar to the GBVTD-retrieved pressure deficit (see text). It is also similar to the pressure deficit measured in similar intensity tornadoes (Winn et al. 1999; Lee et al. 2004). The calculated pressure deficit for a tornado with $V_{\max} = 52$ m s^{-1}, is about 35–40 hPa, which is close to the observed 31–41-hPa drop observed in the Stratford, Texas (2003), tornado, which exhibited a $V_{\max} = 53$ m s^{-1} (Wurman and Samaras 2004). Interestingly, the most intense tropical cyclones with $V_{\max}$ approaching 80 m s^{-1} have achieved pressure deficits of over 120 hPa. This is either due to flatter wind profiles outside of RMW, with $b < 0.4$, or through contributions of the Coriolis terms not being included in the cyclostrophic balance [Eq. (1)]. The pressure deficits of approximately 200 hPa in the extreme cases of $V_{\max} =$ 120 m s^{-1} can be treated as the maximum pressure deficits likely to occur in the most intense tornadoes.

TABLE A1. Pressure deficit (Δp) in hPa at center of atmospheric vortices with various $V_{\max}$ and b when $r_2 = 5$ RMW.

b	$V_{\max} = 120$ m s^{-1}	$V_{\max} = 100$ m s^{-1}	$V_{\max} = 80$ m s^{-1}	$V_{\max} = 60$ m s^{-1}	$V_{\max} = 40$ m s^{-1}
1.0	−165	−115	−73	−41	−18
0.9	−173	−120	−77	−43	−19
0.8	−182	−126	−81	−45	−20
0.7	−192	−133	−85	−48	−21
0.6	−204	−142	−91	−51	−23
0.5	−219	−152	−97	−55	−24
0.4	−237	−164	−105	−59	−26
0.3	−258	−179	−115	−65	−29

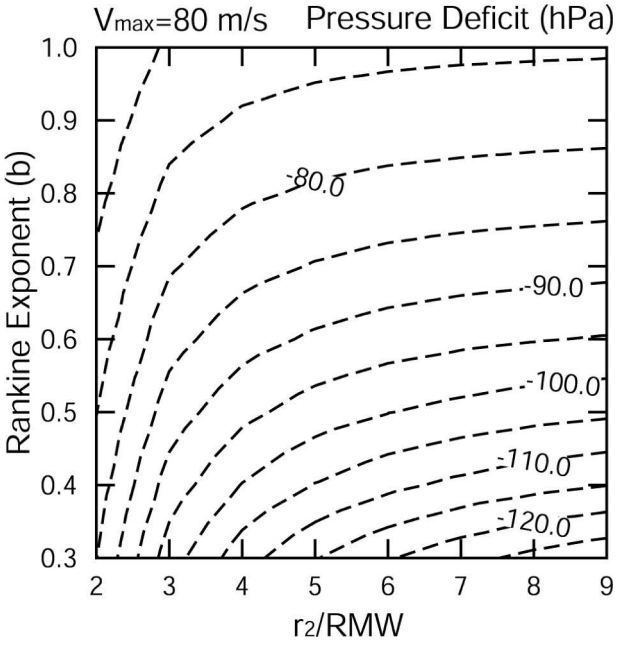

FIG. A1. The pressure deficit (hPa) of a tornado with 80 m s^{-1} maximum mean tangential wind as a function of the exponent of the decay of the wind profile outside of RMW (b) and the ratio of r_2/RMW.

REFERENCES

Alexander, C., and J. Wurman, 2005: The 30 May 1998 Spencer, South Dakota, storm. Part I: The structural evolution and environment of the tornadoes. *Mon. Wea. Rev.,* **133,** 72–96.

Baker, G. L., and C. R. Church, 1979: Measurements of core radii and peak velocities in modeled atmospheric vortices. *J. Atmos. Sci.,* **36,** 2413–2424.

Bell, M., and W.-C. Lee, 2002: An objective method to select a consistent set of tropical cyclone circulation centers derived from the GBVTD-simplex algorithm. Preprints, *25th Conf. on Hurricanes and Tropical Meteorology*, San Diego, CA, Amer. Meteor. Soc., 642–643.

Bluestein, H. B., J. G. LaDue, H. Stein, D. Speheger, and W. P. Unruh, 1993: Doppler radar wind spectra of supercell tornadoes. *Mon. Wea. Rev.,* **121,** 2200–2221.

——, A. L. Pazmany, J. C. Galloway, and R. E. McIntosh, 1995: Studies of the substructure of severe convective storms using a mobile 3-mm-wavelength Doppler radar. *Bull. Amer. Meteor. Soc.,* **76,** 2155–2169.

——, W. P. Unruh, D. C. Dowell, T. A. Hutchinson, T. M. Crawford, C. Wood, and H. Stein, 1997: Doppler radar analysis of the Northfield, Texas, tornado of 25 May 1994. *Mon. Wea. Rev.,* **125,** 212–230.

——, W.-C. Lee, M. Bell, C. Weiss, and A. L. Pazmany, 2003a: Mobile Doppler radar observations of a tornado in a supercell near Bassett, Nebraska, on 5 June 1999. Part II: Tornado vortex structure. *Mon. Wea. Rev.,* **131,** 2955–2984.

——, C. Weiss, and A. L. Pazmany, 2003b: Mobile Doppler radar observations of a tornado in a supercell near Bassett, Nebraska, on 5 June 1999. Part I: Tornadogenesis. *Mon. Wea. Rev.,* **131,** 2954–2967.

Brandes, E. A., 1978: Mesocyclone evolution and tornadogenesis: Some observations. *Mon. Wea. Rev.,* **106,** 995–1011.

——, 1981: Finestructure of the Del City–Edmond tornado mesocirculation. *Mon. Wea. Rev.,* **109,** 635–647.

Brown, R. A., L. R. Lemon, and D. W. Burgess, 1978: Tornado detection by pulsed Doppler radar. *Mon. Wea. Rev.,* **106,** 29–38.

Browning, K. A., and R. Wexler, 1968: The determination of kinematic properties of a wind field using Doppler radar. *J. Appl. Meteor.,* **7,** 105–113.

Burgess, D. W., M. A. Magsig, J. Wurman, D. C. Dowell, and Y. Richardson, 2002: Radar observations of the 3 May 1999 Oklahoma City tornado. *Wea. Forecasting,* **17,** 456–471.

Carbone, R. E., M. J. Carpenter, and C. D. Burghart, 1985: Doppler radar sampling limitations in convective storms. *J. Atmos. Oceanic Technol.,* **2,** 357–361.

——, J. D. Tuttle, D. A. Ahijevych, and S. B. Trier, 2002: Inferences of predictability associated with warm season precipitation episodes. *J. Atmos. Sci.,* **59,** 2033–2056.

Church, C. R., and J. T. Snow, 1985: Measurements of axial pressure in tornado-like vortices. *J. Atmos. Sci.,* **42,** 576–582.

——, ——, G. L. Baker, and E. M. Agee, 1979: Characteristics of tornado-like vortices as a function of swirl ratio: A laboratory investigation. *J. Atmos. Sci.,* **36,** 1755–1766.

Davies-Jones, R. P., 1986: Tornado dynamics. *Thunderstorms: A Social, Scientific and Technological Documentary,* Vol. 2, *Thunderstorm Morphology and Dynamics,* E. Kessler, Ed., University of Oklahoma Press, 197–236.

Dowell, D. C., and H. B. Bluestein, 2002a: The 8 June 1995 McLean, Texas, storm. Part I: Observations of cyclic tornadogenesis. *Mon. Wea. Rev.,* **130,** 2626–2648.

——, and ——, 2002b: The 8 June 1995 McLean, Texas, storm. Part II: Cyclic tornado formation, maintenance, and dissipation. *Mon. Wea. Rev.,* **130,** 2649–2670.

——, Y. P. Richardson, and J. Wurman, 2002: Observations of the formation of low-level rotation: The 5 June 2001 Summer County, Kansas, tornado. Preprints, *21st Conf. on Severe Local Storms*, San Antonio, TX, Amer. Meteor. Soc., 465–468.

——, C. Alexander, J. Wurman, and L. Wicker, 2005: Centrifuging of hydrometers and debris in tornadoes: Radar-reflectivity patterns and wind-measurement errors. *Mon. Wea. Rev.,* **133,** 1501–1524.

Fiedler, B. H., 1993: Numerical simulation of axisymmetric tornadogenesis in buoyant convection. *The Tornado: Its Structure, Dynamics, Prediction, and Hazards, Geophys. Monogr.,* No. 79, American Geophysical Union, 41–48.

——, and R. Rotunno, 1986: A theory for the maximum windspeeds in tornado-like vortices. *J. Atmos. Sci.,* **43,** 2328–2340.

Folkard, C., 2005: *Guinness World Records 2005*. Bantam, 288 pp.

Fujita, T. T., 1970: The Lubbock tornadoes: A study of suction spots. *Weatherwise,* **23,** 160–173.

——, and A. D. Pearson, 1973: Results of FPP classification of 1971 and 1972 tornadoes. Preprints, *Eighth Conf. on Severe Local Storms*, Denver, CO, Amer. Meteor. Soc., 142–145.

——, D. L. Bradbury, and C. F. Van Thullenar, 1970: Palm Sunday tornadoes of April 11, 1965. *Mon. Wea. Rev.,* **98,** 29–69.

Gal-Chen, T., 1978: A method for the initialization of the anelastic equations for matching models with observations. *Mon. Wea. Rev.,* **106,** 587–606.

Gall, R. L., 1983: A linear analysis of the multiple vortex phenomenon in simulated tornadoes. *J. Atmos. Sci.,* **40,** 2010–2024.

Golden, J. H., and D. Purcell, 1978: Airflow characteristics around the Union City tornado. *Mon. Wea. Rev.,* **106,** 22–28.

Hoecker, W. H., 1960: Wind speed and air flow patterns in the Dallas tornado of April 2, 1957. *Mon. Wea. Rev.,* **88,** 167–180.

Holton, J. R., 1979: *An Introduction to Dynamic Meteorology.* 2d ed. Academic Press, 391 pp.

Klemp, J. B., and R. Rotunno, 1983: A study of the tornado region within a supercell thunderstorm. *J. Atmos. Sci.,* **40,** 359–377.

Lee, J. J., T. Samaras, and C. Young, 2004: Pressure measurements at the ground in an F-4 tornado. Preprints, *22d Conf. on Severe Local Storms,* Hyannis, MA, Amer. Meteor. Soc., CD-ROM, 15.3.

Lee, W.-C., and F. D. Marks, 2000: Tropical cyclone kinematic structure retrieved from single Doppler radar observations. Part II: The GBVTD-simplex center finding algorithm. *Mon. Wea. Rev.,* **128,** 1925–1936.

——, ——, and R. E. Carbone, 1994: Velocity Track Display (VTD)—A technique to extract primary vortex circulation of a tropical cyclone in real-time using single airborne Doppler radar data. *J. Atmos. Oceanic Technol.,* **11,** 337–356.

——, J.-D. Jou, P.-L. Chang, and S.-M. Deng, 1999: Tropical cyclone kinematic structure retrieved from single Doppler radar observations. Part I: Interpretation of Doppler velocity patterns and the GBVTD technique. *Mon. Wea. Rev.,* **127,** 2419–2439.

——, ——, ——, and F. D. Marks, 2000: Tropical cyclone kinematic structure retrieved from single-Doppler radar observations. Part III: Evolution and structure of Typhoon Alex (1987). *Mon. Wea. Rev.,* **128,** 3982–4001.

Letzmann, J., 1923: Das Bewegungsfeld im Fuss einer fortschreitenden Wind- oder Wasserhose (The flow field at the base of a progressing tornado). Ph.D. thesis, University of Dorpat, 80 pp. [Available online at www.essl.org/pdf/Letzmann1923/Letzmann1923.pdf.]

Lewellen, W. S., 1976: Theoretical models of the tornado vortex. *Proc. Symp. on Tornadoes, Assessment of Knowledge and Implications for Man,* Lubbock, TX, 107–144.

——, D. C. Lewellen, and R. I. Sykes, 1997: Large-eddy simulation of a tornado's interaction with the surface. *J. Atmos. Sci.,* **54,** 581–605.

——, ——, and J. Xia, 2000: The influence of a local swirl ratio on tornado intensification near the surface. *J. Atmos. Sci.,* **57,** 527–544.

Mallen, K. J., M. T. Montgomery, and B. Wang, 2005: Re-examining tropical cyclone near-core radial structure using aircraft observations: Implications for vortex resiliency. *J. Atmos. Sci.,* **62,** 408–425.

Marks, F. D., R. A. Houze, and J. F. Gamache, 1992: Dual-aircraft investigation of the inner core of Hurricane Norbert. Part I: Kinematic structure. *J. Atmos. Sci.,* **49,** 919–942.

Marshall, T., 2004: The enhanced Fujita (EF) scale. Preprints, *22d Conf. on Severe Local Storms*, Hyannis, MA, Amer. Meteor. Soc., CD-ROM, 3B.2.

Oye, R., C. Mueller, and S. Smith, 1995: Software for radar data translation, visualization, editing, and interpolation. Preprints, *27th Conf. on Radar Meteorology,* Vail, CO, Amer. Meteor. Soc., 359–361.

Pauley, R. L., 1989: Laboratory measurements of axial pressure in two-celled tornado-like vortices. *J. Atmos. Sci.,* **46,** 3392–3399.

——, C. R. Church, and J. T. Snow, 1982: Measurements of maximum pressure deficits in modeled atmospheric vortices. *J. Atmos. Sci.,* **39,** 369–377.

Peterson, R. E., 1992a: Johannes Letzmann: A pioneer in the study of tornadoes. *Wea. Forecasting,* **7,** 166–184.

——, 1992b: Letzmann's and Koschmieder's "Guidelines for research on funnels, tornadoes, waterspouts and whirlwinds." *Bull. Amer. Meteor. Soc.,* **73,** 597–611.

Richardson, Y. P., D. C. Dowell, J. M. Wurman, P. Zhang, and S. Weygandt, 2001: Preliminary high-resolution dual-Doppler analyses of two tornadic thunderstorms. Preprints, *30th Int. Conf. on Radar Meteorology,* Munich, Germany, Amer. Meteor. Soc., 295–297.

Roberts, R. D., and J. W. Wilson, 1995: The genesis of three nonsupercell tornadoes observed with dual-Doppler radar. *Mon. Wea. Rev.,* **123,** 3408–3436.

Rotunno, R., 1977: Numerical simulation of a laboratory vortex. *J. Atmos. Sci.,* **34,** 1942–1956.

——, 1979: A study in tornado-like vortex dynamics. *J. Atmos. Sci.,* **36,** 140–155.

——, 1986: Tornadoes and tornadogenesis. *Mesoscale Meteorology and Forecasting*, P. Ray, Ed., Amer. Meteor. Soc., 414–436.

——, and K. Emanuel, 1987: An air–sea interaction theory for tropical cyclones. Part II: Evolutionary study using a nonhydrostatic axisymmetric numerical model. *J. Atmos. Sci.,* **44,** 542–561.

Roux, F., and F. D. Marks Jr., 1996: Extended Velocity Track Display (EVTD): An improved processing method for Doppler radar observations of tropical cyclones. *J. Atmos. Oceanic Technol.,* **13,** 875–899.

Snow, J. T., 1978: On inertial instability as related to the multiple-vortex phenomenon. *J. Atmos. Sci.,* **35,** 1660–1677.

——, 1982: A review of recent advances in tornado vortex dynamics. *Rev. Geophys. Space Phys.,* **20,** 953–964.

——, and R. L. Pauley, 1984: On the thermodynamic method for estimating maximum tornado windspeeds. *J. Climate Appl. Meteor.,* **23,** 1465–1468.

——, C. R. Church, and B. J. Barnhart, 1980: An investigation of the surface pressure fields beneath simulated tornado cyclones. *J. Atmos. Sci.,* **37,** 1013–1026.

Speheger, D. A., C. A. Doswell, and G. J. Stumpf, 2002: The tornadoes of 3 May 1999: Event verification in central Oklahoma and related issues. *Wea. Forecasting,* **17,** 362–381.

Staley, D. O., and R. L. Gall, 1979: Barotropic instability in a tornado vortex. *J. Atmos. Sci.,* **36,** 973–981.

——, and ——, 1984: Hydrodynamic instability of small eddies in a tornado vortex. *J. Atmos. Sci.,* **41,** 422–429.

Wakimoto, R. M., and B. E. Martner, 1992: Observations of a Colorado tornado. Part II: Combined photogrammetric and Doppler radar analysis. *Mon. Wea. Rev.,* **120,** 522–543.

——, and C.-W. Liu, 1998: The Garden City, Kansas, storm during VORTEX 95. Part II: The wall cloud and tornado. *Mon. Wea. Rev.,* **126,** 393–408.

——, and H. Cai, 2000: Analysis of a nontornadic storm during VORTEX 95. *Mon. Wea. Rev.,* **128,** 565–592.

——, W.-C. Lee, H. B. Bluestein, C.-H. Liu, and P. H. Hildebrand, 1996: ELDORA observations during VORTEX 1995. *Bull. Amer. Meteor. Soc.,* **77,** 1465–1481.

——, C.-W. Liu, and H. Cai, 1998: The Garden City, Kansas, storm during VORTEX 95. Part I: Overview of the storm's life cycle and mesocyclogenesis. *Mon. Wea. Rev.,* **126,** 372–392.

Walko, R. L., 1988: Plausibility of substantial dry adiabatic subsidence in a tornado core. *J. Atmos. Sci.,* **45,** 2251–2267.

Ward, N. B., 1972: The exploration of certain features of tornado dynamics using a laboratory model. *J. Atmos. Sci.,* **29,** 1194–1204.

Willoughby, H. E., J. A. Clos, and M. G. Shoreibah, 1982: Concentric eyewalls, secondary wind maxima, and the evolution of the hurricane vortex. *J. Atmos. Sci.,* **39,** 395–411.

Winn, W. P., S. J. Hunyady, and G. D. Aulich, 1999: Pressure at the ground in a large tornado. *J. Geophys. Res.,* **104D,** 22 067–22 082.

Wurman, J., 1999: Preliminary results from the Radar Observations of Tornadoes and Thunderstorms Experiment (ROTATE-98/99). Preprints, *29th Conf. on Radar Meteorology,* Montreal, QC, Canada, Amer. Meteor. Soc., 613–616.

——, 2001: The DOW mobile multiple Doppler network. Preprint, *30th Int. Conf. on Radar Meteorology,* Munich, Germany, Amer. Meteor. Soc., 95–97.

——, 2002: The multiple vortex structure of a tornado. *Wea. Forecasting,* **17,** 473–505.

——, and S. Gill, 2000: Finescale radar observations of the Dimmitt, Texas (2 June 1995), tornado. *Mon. Wea. Rev.,* **128,** 2135–2164.

——, and M. Randall, 2001: An inexpensive, mobile, Rapid-Scan Radar. Preprints, *30th Conf. on Radar Meteorology,* Munich, Germany, Amer. Meteor. Soc., 98–100.

——, and C. Alexander, 2004: Scales of motion in tornadoes, what radars cannot see, what scale circulation is a tornado. *Proc. 22d Conf. on Severe Local Storms*, Hyannis, MA, Amer. Meteor. Soc., CD-ROM, P11.6.

——, and T. Samaras, 2004: Comparison of in-situ and DOW Doppler winds in a tornado and RHI vertical slices through 4 tornadoes during 1996–2004. Preprints, *22d Conf. on Severe Local Storms*, Hyannis, MA, Amer. Meteor. Soc., CD-ROM, 15.4.

——, and C. Alexander, 2005: The 30 May 1998 Spencer, South Dakota, storm. Part II: Comparison of observed damage and radar-derived winds in the tornadoes. *Mon. Wea. Rev.,* **133,** 97–119.

——, J. M. Straka, E. N. Rasmussen, M. Randall, and A. Zahrai, 1997: Design and deployment of a portable, pencil-beam, pulsed, 3-cm Doppler radar. *J. Atmos. Oceanic Technol.,* **14,** 1502–1512.